



A drier Orinoco basin during the twenty-first century: the role of the Orinoco low-level jet

Isabel C. Correa¹ · Paola A. Arias¹ · Sara C. Vieira¹ · J. Alejandro Martínez²

Received: 24 March 2023 / Accepted: 16 November 2023 / Published online: 4 January 2024
© The Author(s) 2024

Abstract

This study focuses on the analysis of the simulation of the main climatological features of the Orinoco low-level jet (OLLJ) by a set of models included in the Sixth Phase of the Coupled Model Intercomparison Project (CMIP6) and their projected changes under three Shared Socioeconomic Pathways (SSPs): SSP2-4.5, SSP3-7.0, and SSP5-8.5. We consider the 1979–2014 period to evaluate the historical simulations using the ERA5 reanalysis as the reference dataset. In general, CMIP6 models are able to capture the activation of the OLLJ during December–January–February (DJF) in the Orinoco basin, as well as the main links between this circulation and low-level moisture transport patterns in northern South America. Regarding the analysis of projections, CMIP6 models suggest a weakening and shrinking of the OLLJ, especially in its exit region, by the end of the twenty-first century, which in turn induces changes in atmospheric moisture transport patterns in the region during DJF. The projected changes of the OLLJ are associated with variations in the regional gradients of mean sea level pressure, near-surface air temperature, and surface sensible heat flux in association with drier conditions in the Orinoco basin. These projections are consistent with previous studies suggesting a drier Orinoco river basin throughout the twenty-first century. Assessing the projected changes of this low-level jet in northern South America improves our understanding of the different phenomena that modulate atmospheric moisture transport in the region, which is particularly important given its high vulnerability to climate change.

Keywords Orinoco low-level jet · Northern South America · CMIP6 · Projections · Regional gradients

1 Introduction

The water cycle has experienced variations worldwide associated with global climate change, inducing significant variability in the Earth system components. Atmospheric, oceanic, and terrestrial processes are interconnected, giving a high complexity to the global and regional hydrological cycle and its understanding under different conditions (Douville et al. 2021; Yang et al. 2021). One of the main drivers of changes in the water cycle is the rise in the tropospheric air temperatures (e.g. Al-Ghussain 2019; Gulev et al. 2021), causing noticeable changes in weather and climatological

phenomena, and in turn, leading to the intensification of the water cycle (Barichivich et al. 2018; Allan et al. 2020; Douville et al. 2021). This means that weather and climate extremes are becoming more frequent and intense and that the seasonality of the water cycle is increasing (Douville et al. 2021; Seneviratne et al. 2021).

Water vapor transport through the atmosphere plays a relevant role in the hydrological cycle. It allows the exchange of water vapor between sources and sinks, enhancing precipitation formation and the maintenance of ecosystems (Gimeno et al. 2012, 2020; Herrera-Estrada et al. 2019). For instance, water vapor from the oceans and terrestrial sources plays an essential role in the generation of precipitation events around the world and is expected to strongly influence the changes in precipitation extremes as a response to fluctuations in moisture sources and their transport mechanisms (Liu et al. 2020). However, the particularities of those changes depend on the region, the season, and the features that modulate the moisture-related processes (e.g. Gimeno et al. 2012; Liu et al. 2020). Atmospheric rivers and low-level jets (LLJs) are

✉ Isabel C. Correa
isabel.correas@udea.edu.co

¹ Grupo de Ingeniería y Gestión Ambiental (GIGA),
Escuela Ambiental, Facultad de Ingeniería, Universidad de
Antioquia, Medellín, Colombia

² Escuela Ambiental, Facultad de Ingeniería, Universidad de
Antioquia, Medellín, Colombia

known as two effective mechanisms of moisture transport (e.g. Poveda et al. 2014; Arias et al. 2015; Gimeno et al. 2016; Acosta and Huber 2017; Gallego et al. 2019; Morales et al. 2021; Munday et al. 2021; Makinde et al. 2022; Oscar et al. 2022) whose role in the formation of extreme weather events have been analyzed in previous studies (e.g. Gimeno et al. 2016; Ramos et al. 2016, 2019; Gimeno-Sotelo et al. 2022; Gimeno-Sotelo and Gimeno 2023). In particular, increases in atmospheric moisture transport during the last decades have triggered more extreme weather events, either in terms of intense precipitation or droughts (Bonner 1968; Stensrud 1996; Poveda et al. 2014; Gimeno et al. 2016; Douville et al. 2021).

The influence of LLJs on the regional water cycle over northern South America has been previously addressed, particularly the Choco LLJ (Poveda and Mesa 1999), the Caribbean LLJ (Amador 1998, 2008), and the Orinoco LLJ (OLLJ; Torrealba and Amador 2010). The Caribbean and Choco LLJs have received important attention regarding their main features and variability (e.g., Poveda and Mesa 1999; Wang 2007; Whyte et al. 2007; Amador 2008; Muñoz et al. 2008; Cook and Vizy 2010; Sierra et al. 2018, 2021b; Yepes et al. 2019; Loaiza-Cerón et al. 2020; Morales et al. 2021; Valencia and Mejía 2022) while the OLLJ has been less studied.

The different studies assessing the OLLJ highlight the relevance of this LLJ on atmospheric moisture transport and, therefore, the hydrological cycle in northern South America. Poveda and Mesa (1999) identified this jet from an earlier generation of reanalyses, finding a strengthening of the low-level wind field in the eastern Andes Mountain range of northern South America. Later studies evaluate the seasonal characteristics of the OLLJ, suggesting a stronger jet during December–January–February (DJF; Montoya et al. 2001; LaBar et al. 2005; Rueda 2014), which corresponds to the dry season in the Orinoco basin (e.g., Arias et al. 2020). Different ranges of pressure levels have been associated with the seasonal activation of the jet; however, this jet is always confined between 1000 and 800 hPa, consistent with the behavior of a LLJ. Builes-Jaramillo et al. (2022b) analyzed the interannual variability of the OLLJ associated with the El Niño–Southern Oscillation (ENSO). Particularly, they identified that the OLLJ winds decrease (increase) over the mid and exit regions of the OLLJ corridor during the occurrence of El Niño (La Niña) events. These changes are modulated by decreases (increases) in the surface pressure gradient between the North Atlantic Subtropical High (NASH) and

the near-equatorial low-pressure regions during El Niño (La Niña), inducing a decrease (increase) of the OLLJ intensity.

Some studies link the OLLJ with regional phenomena, such as the transport of pollutants from the Atlantic Ocean and the Orinoco basin to central Colombia and Ecuador during February–March–April (Rodríguez-Gómez et al. 2022). In terms of the link between the OLLJ, precipitation, and atmospheric moisture transport patterns in northern South America, Labar et al. (2005) found that during the dry season in the Orinoco basin (DJF), deep convection occurs in southern Colombia but does not occur in the jet corridor through the Venezuelan Llanos.

Nieto et al. (2008) suggest that most of the water over the Orinoco basin derives from advective fluxes into the area while the recycling of moisture is negligible. Moreover, Algarra et al. (2019) used a regional model to track the atmospheric moisture sources and sinks of different nocturnal LLJs, suggesting that the OLLJ plays a relevant role in water vapor transport from the tropical north Atlantic Ocean to the northwestern Amazon. Builes-Jaramillo et al. (2022a) linked the OLLJ with moisture flux and precipitation in northern South America from composite analysis during the period of activation (DJF) and the period of non-activity of the jet (June–July–August; JJA). Their results indicate that during DJF, precipitation increases south of the exit region of the jet while the moisture flux on the Orinoco basin is enhanced. On the contrary, in JJA, when the jet activity decreases, the main low-level circulation in the region is associated with the southerly cross-equatorial flow from the Amazon basin. Martinez et al. (2022) found that higher surface sensible heat flux and lower evaporation in the entrance of the jet can lead to the weakening of the wind flow and decreases in the cross-equatorial moisture transport into the Amazon linked to the OLLJ activity. The above suggests the role of the OLLJ on atmospheric moisture flux from the tropical north Atlantic Ocean to the Amazon basin in DJF and its interactions with the regional circulation.

Like other regions worldwide, South America, specifically northern South America, has experienced relevant changes in its climatological characteristics that lead to variations in the structure of regional ecosystems and human systems over the region (Castellanos et al. 2022). For instance, Chai et al. (2021) identify drier conditions in central South America after analyzing aridity trends during 1965–2014, while Mesa et al. (2021) show an intensification of the hydrological cycle in Colombia (northwestern South America), with drier conditions over the Orinoco. The most

recent assessment report of the Intergovernmental Panel on Climate Change (IPCC) shows that heavy precipitation events have increased in frequency and intensity over southeastern South America while agricultural and ecological droughts have become more frequent in northeastern South America (Arias et al. 2021a; IPCC 2021; Seneviratne et al. 2021). These conditions may become more severe under future climate change induced by increasing greenhouse gas (GHG) concentrations (IPCC 2021).

The changes in atmospheric moisture transport toward and within northern South America are particularly relevant to understand the projected changes in the regional hydrological cycle, due to the complexity of the transport patterns of atmospheric moisture (e.g. Poveda et al. 2014; Arias et al. 2015, 2023; Hoyos et al. 2018; Agudelo et al. 2019) and the interhemispheric exchange that occurs in the region (e.g. Martinez et al. 2022). Specifically, the analysis of climate projections from General Circulation Models (GCMs) for northern South America suggests shifts in the location and strengthening of the Choco LLJ during September–October–November, as a result of changes in the temperature and pressure gradients between the eastern tropical Pacific Ocean and the Colombian landmass (Sierra et al. 2021a), which can also influence regional precipitation (Valencia and Mejía 2022). Other projections suggest a westward expansion of the Caribbean LLJ, partially explained by the dynamics of the NASH (Torres-Alavez et al. 2021). By contrast, the possible changes of the OLLJ under climate change scenarios have not been addressed in the literature.

Therefore, this study focuses on the evaluation of GCMs simulating the main features of the OLLJ and their projected changes by the end of the twenty-first century. The above acquires relevance due to the role of the OLLJ in the atmospheric circulation in northern South America. This paper is structured as follows: Sect. 2 describes the data and methodology used, Sect. 3 discusses the main results, and finally, Sect. 4 presents a summary and discussion from this work.

2 Data and methodology

2.1 Climatological features of the OLLJ

This study uses the European Centre for Medium-Range Weather Forecasts reanalysis ERA5 (Hersbach et al. 2020) to describe the main characteristics of the OLLJ during 1979–2014, which is the common period with the GCMs used (see Sect. 2.2). ERA5 corresponds to a state-of-the-art reanalysis and has a horizontal resolution of $0.25^\circ \times 0.25^\circ$. Previous studies have used this reanalysis as a reference to evaluate GCMs simulations in South America (e.g. Arias et al. 2021c; Ortega et al. 2021; Olmo et al. 2022). Other

studies have highlighted the improvements of ERA5 over another reanalysis in the representation of hydrological and atmospheric variables although maintaining some biases, such as the overestimation of the temperature in southern South America (Albergel et al. 2018; Tarek et al. 2020; BalmacedaHuarte et al. 2021).

To analyze the main seasonal features of this LLJ, we use monthly zonal and meridional winds at different pressure levels over northern South America (20°N – 10°S , 85 – 50°W). In particular, we analyze the seasonal vertical structure of the wind field, and the seasonal spatial distribution of the horizontal wind.

In addition to the seasonal wind fields, we propose an index to assess the wind variability in the Orinoco basin associated with the activation of the OLLJ. We define the OLLJ index as the spatial average of the horizontal wind between the levels of 825 and 950 hPa over the region 3° – 5°N , 73° – 67°W (region C3.4; solid black rectangle in Fig. 1). This domain is chosen given that previous studies estimate indices over much smaller regions that may not be appropriate when considering GCMs (e.g. Jiménez-Sánchez et al. 2019, 2020; Martinez et al. 2022). Particularly, Rodríguez-Gómez et al. (2022) use the region 75° – 61°W , 4°N to analyze the vertical structure of the OLLJ. However, as the OLLJ index used in this study considers the average wind

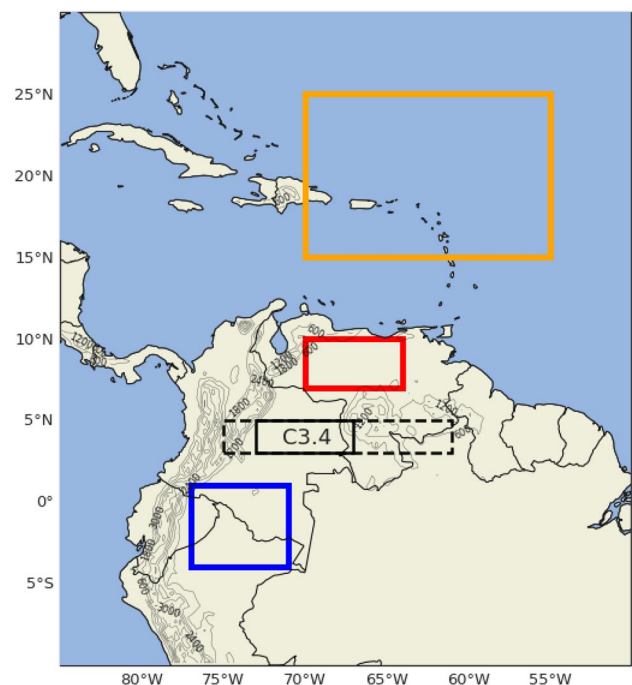


Fig. 1 Regions considered to evaluate the simulation of the main OLLJ characteristics by the General Circulation Models used: region C3.4 (black), Tropical North Atlantic (orange), Orinoco (red), and Andes-Amazon transition (blue). The dashed black rectangle corresponds to the region considered to estimate vertical cross-sections, and black contours represent the topography in meters

field over a spatial domain, a region including a wide range of longitudinal bands that do not correspond to the main developing domain of this jet may bias the index estimate. Therefore we restricted the index domain to the region C3.4 shown in the solid rectangle of Fig. 1.

2.2 MSLP and NSAT gradients between the ocean and the landmass

We evaluate the monthly variation of the gradients of mean sea level pressure (MSLP) and near-surface air temperature (NSAT) between the Tropical North Atlantic and the Amazon, since the contrast in pressure and heating between these regions is related to the activation of the OLLJ (Builes-Jaramillo et al. 2022b; Martínez et al. 2022). These gradients are calculated as the difference between the spatial average of the MSLP and NSAT in the Tropical North Atlantic (70° W–55° W, 15° N–25° N; orange rectangle in Fig. 1) and the Andes-Amazon transition (72° W–77° W, 4° S–1° N; blue rectangle in Fig. 1; Martínez et al. 2022). As for the case of the wind fields, we consider ERA5 as the reference dataset for these estimates.

2.3 Regional gradients of MSLP, NSAT and SSHF over the continent

On the other hand, this study analyzes the representation of the MSLP, Surface Sensible Heat Flux (SSHF), and NSAT gradients between the Orinoco (64°–70° W, 7°–10° N; red rectangle in Fig. 1) and the Andes-Amazon transition regions (blue rectangle in Fig. 1; Martínez et al. 2022). This is relevant because the regional gradients between the jet entrance and exit regions are important for interannual variations of the OLLJ intensity. We use ERA5 as the reference dataset for these estimates.

We consider the time series of the long-term anomaly of the OLLJ index during DJF to identify the years of strong and weak jet periods. We define the occurrence of a strong jet event when the anomaly is above one standard deviation of the long-term series. On the contrary, a weak jet event is defined from the anomalies that are below one standard deviation. Finally, to assess the main changes during strong and weak events, we evaluate the patterns of MSLP, NSAT and SSHF gradients, estimated as the difference between the Orinoco region and the Andes-Amazon transition region for those specific events.

2.4 Links between the OLLJ and atmospheric moisture patterns in northern South America

Finally, we propose an initial approach to understand the role of the OLLJ in the seasonal atmospheric moisture transport in northern South America using zonal and meridional wind data and specific humidity in different pressure levels at a monthly time scale. For this purpose, we estimate the vertically integrated moisture flux (VIMF) using Eq. 1:

$$VIMF = \frac{1}{g} \int_{pl}^{pu} Vqdp \quad (1)$$

where V represents the wind vector in m/s, q is the specific humidity in kg/kg, and pu and pl are the upper and lower pressure levels in Pa, and g is the acceleration due to gravity.

The relationship between VIMF and the jet activity is identified through a simple linear regression between the monthly anomalies of the OLLJ index and the anomalies of the VIMF at each grid cell of the spatial domain.

2.5 Model evaluation

We analyze the annual cycle of the OLLJ using the historical simulations of 34 GCMs included in the sixth phase of the Coupled Model Intercomparison Project (CMIP6; Eyring et al. 2016). We only consider the first model initialization for these simulations (r1i1p1f1). CMIP6 models are evaluated using the ERA5 reanalysis, which is available for the period 1940–present. However, the period of analysis of the historical experiment in this study corresponds to 1979–2014. Table S1 presents the models used in this analysis, their spatial resolution, and available experiments.

The simulation of the main features of the OLLJ by the considered CMIP6 models is evaluated using the monthly OLLJ index (see Sect. 2.1), the seasonal vertical structure of the wind field, and the seasonal spatial distribution of the horizontal wind. We also evaluate how the CMIP6 models simulate the regional patterns of MSLP, NSAT, SSHF, and VIMF. Therefore the variables used from the GCMs are zonal and meridional wind components, specific humidity, sea-level pressure, NSAT, and SSHF.

Following the methodology proposed by Sierra et al. (2018), we use the Root Mean Square Error (RMSE) and the pattern correlation coefficient (PCC) as the evaluation metrics of the performance of each model in the simulation of the observed seasonal characteristics of the OLLJ (Taylor

2001). For calculating the evaluation metrics, ERA5 data is interpolated to each model grid size (Table S1) by bilinear interpolation. Then, to classify the set of CMIP6 models according to their ability to simulate seasonal variations of the wind field in northern South America, we perform a factor analysis using RMSE and PCC. From this methodology, it is possible to obtain a small number of factors that explain most of the original variance and allows the reduction of the number of variables to classify the models (Rencher 2003; Sierra et al. 2018). Finally, we use cluster analysis to obtain a grouping of the CMIP6 models from the factors selected by the factor analysis. In this sense, cluster analysis is a statistical technique that allows defining groups of a set of individuals, thus the individuals within a cluster are similar while they tend to differ from those classified in other groups (Wilks 2006). After obtaining the groups, we focus on how each cluster represents the main characteristics of the OLLJ. The models within each cluster are gridded to a common grid size of $2^\circ \times 2^\circ$ by bilinear interpolation to obtain the multimodel mean of the horizontal wind patterns, the vertical structure of the jet, and the OLLJ index for each cluster of GCMs.

To analyze the twenty-first century projections of the main features of the OLLJ, the models used are defined by the availability of the variables for the different Shared Socioeconomic Pathways (SSPs; Riahi et al. 2017) considered. To assess the projected changes of the OLLJ, this study uses the SSP2-4.5, SSP3-7.0, and SSP5-8.5, which correspond to low, intermediate, and high GHG emission scenarios, respectively (Riahi et al. 2017; Meinshausen et al. 2020). The projected changes of the horizontal wind field are evaluated using the differences between the multimodel mean for projections during 2081–2100 (late twenty-first century) and the historical simulations during 1979–2014.

In addition, we analyze the projected changes in the jet intensity using the OLLJ index, aiming to identify possible changes in the jet strength during its activation period (DJF) throughout the twenty-first century. The projected changes of the OLLJ index are calculated from the DJF historical climatology. We also perform a trend analysis of the long-term series using the Mann–Kendall test (Mann 1945; Kendall 1948), which is a non-parametric test widely used in the detection of trends of atmospheric variables.

3 Results

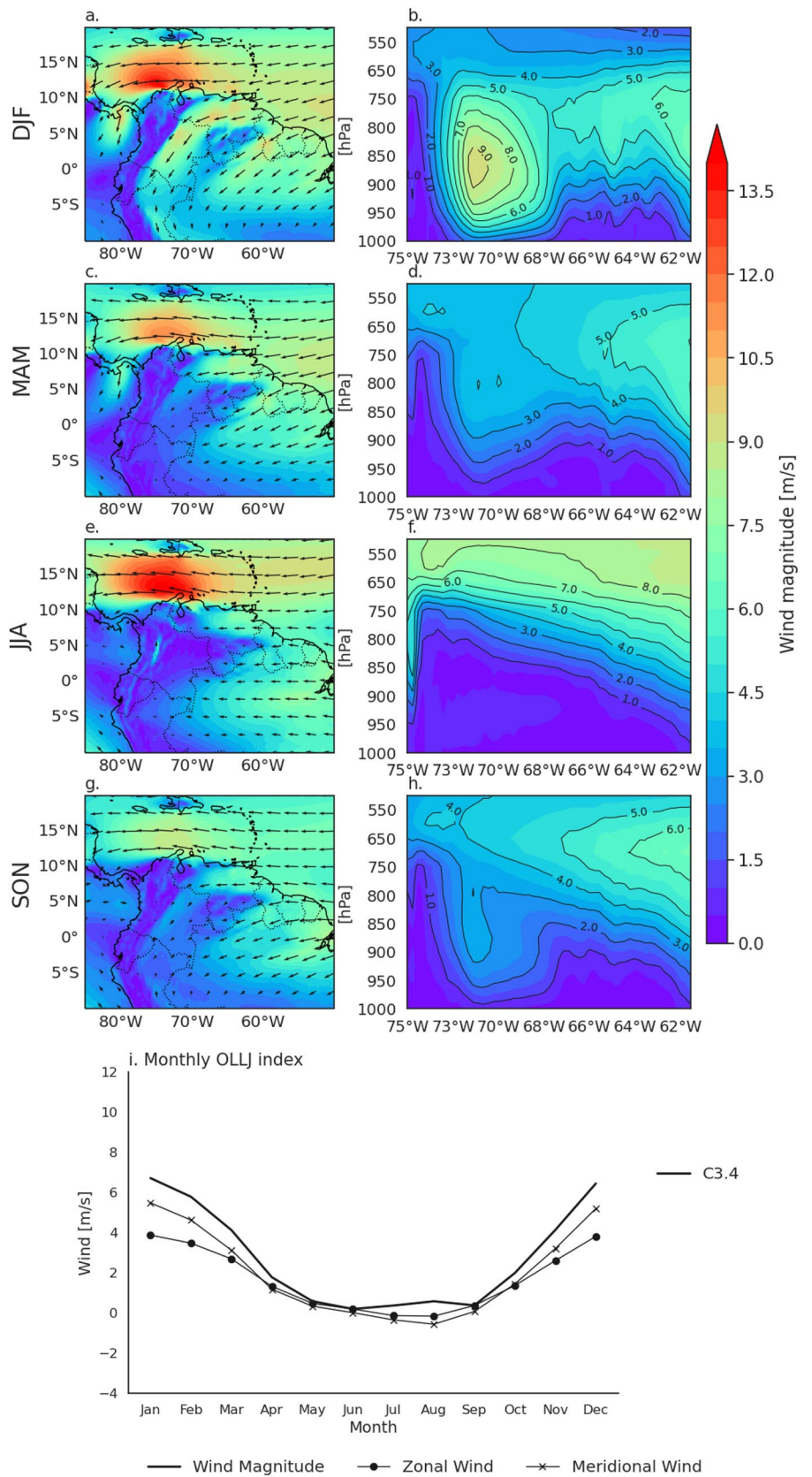
3.1 Climatological features of the OLLJ from ERA5

Figure 2 shows the seasonal patterns of horizontal winds between 925 and 850 hPa over northern South America. During DJF, the wind field experiences a strengthening through the Orinoco basin, reaching the Colombian Amazon (Fig. 2a). In March–April–May (MAM), the wind field reduces its magnitude and the region with strong winds shrinks (Fig. 2c) until it reaches its minimum during JJA (Fig. 2e). The precipitation regime in the Orinoco basin consists of an unimodal regime, with its dry season in DJF and a wet season in JJA (e.g., Urrea et al. 2019; Arias et al. 2020; Builes-Jaramillo et al. 2022a). Accordingly, ERA5 shows a marked annual cycle of the OLLJ with full development and maximum spatial extension during the dry season of the Orinoco basin (DJF) and with its weakest period during the wet season in the basin (JJA).

Figure 2 also shows the seasonal variation of the horizontal wind field associated with the OLLJ and its vertical structure at the jet exit ($75\text{--}61^\circ$ W, $3^\circ\text{--}5^\circ$ N; see Fig. 1), highlighting the difference in the vertical structure of the OLLJ during the activation (DJF) and weakening (JJA) phases of this low-level circulation. Figure 2b indicates that the wind field in the Colombian Llanos experiences a strengthening during DJF, exhibiting a development of the vertical structure of the jet with its core below 800 hPa. The jet centered at 4° N seems to develop between 73 and 67° W and this location is strongly influenced by the regional topography, allowing the strengthening of the wind field between the Los Andes mountain range and the Guinea highlands.

In JJA (Fig. 2f), the wind field decreases its magnitude to values lower than 1 m/s below 800 hPa, indicating the period of weakest activity of the OLLJ. Finally, in September–October–November (SON; Fig. 2h), the wind magnitudes approximately at 900 hPa increase, marking the activation of the OLLJ. The spatial distribution of the wind field associated with the OLLJ is characterized by the change in the wind direction when crossing the South American landmass, mainly driven by the regional topography (see Fig. 1). At its entrance, the jet has a strong zonal direction, while at its exit, the low-level wind speed has substantial

Fig. 2 a, c, e, g Climatological mean horizontal wind between 825 and 950 hPa in northern South America estimated from ERA5 data during 1979–2019. **b, d, f, h** Vertical structure of the wind field at the exit of the Orinoco low-level jet (OLLJ), estimated over the dashed-line region shown in Fig. 1. **(i)** Annual cycle of the OLLJ index estimated in the region C3.4



contributions from both components of the horizontal wind vector field. The OLLJ index estimated in region C3.4 (Fig. 2i) shows that both the zonal and meridional wind components exhibit larger values in DJF and smaller values in JJA, similar to the behavior of the OLLJ. Therefore, both wind components contribute to the resultant wind magnitude. It is relevant to mention that the OLLJ index uses the spatial average of the horizontal wind speed in a range of pressure levels (between 825 and 950 hPa) as a proxy of the jet activity, which is helpful to evaluate climatological features of the jet; however, this approach does not measure other characteristics as the occurrence of specific jet events or its vertical structure.

Martinez et al. (2022) suggest that surface fluxes influence the pressure gradients between the northern Orinoco and the Andes-Amazon transition region. Hence, we evaluate the influence of these regional gradients in the strengthening and weakening of the flow associated with the OLLJ. Figure 3a, b present the climatological fields of the MSLP and SSHF for DJF, showing that the Venezuelan Llanos exhibit higher values of MSLP during this season in comparison to the southernmost region of the OLLJ corridor. On the contrary, the Andes-Amazon transition region (blue rectangle), located at the jet exit, exhibits lower pressure values on the surface during DJF. On the other hand, the SSHF over the Orinoco region (red rectangle) is higher than over the Andes-Amazon transition zone, which is strongly influenced by the hydroclimatological characteristics of each area: the Llanos are characterized by drier conditions where the typical vegetation is grassland, while on the contrary, the Andes-Amazon transition zone has a more humid regime characterized by higher amounts of precipitation and soil moisture (e.g., San José et al. 1998; Arias et al. 2020; Espinoza et al. 2020; Martinez et al. 2022).

In addition, we evaluate the regional patterns of the MSLP and SSHF gradients during strong and weak OLLJ events (see Sect. 2.3). We focus on the period DJF because it corresponds to the strongest jet activity. Figure 3d–f show the time series of anomalies of the OLLJ index for DJF and the gradients of MSLP and SSHF between the Orinoco (red rectangle in Fig. 1) and the Andes-Amazon transition (blue rectangle in Fig. 1) regions during 1979–2019. Additionally, the bottom panel (Fig. 3g) shows the NSAT gradients in order to relate changes in SSHF and MSLP gradients to changes in NSAT. The red (blue) lines correspond to strong (weak) OLLJ events in DJF, and the dashed red (blue) lines indicate La Niña (El Niño) conditions during that year. A stronger OLLJ tends to be accompanied by stronger MSLP and weaker SSHF gradients between the Orinoco and the

Andes-Amazon transition region. On the contrary, a weaker OLLJ is accompanied by a weaker MSLP and a stronger SSHF gradient between these two regions. This can be explained since a greater SSHF in the Orinoco region is related to an increase in NSAT that decreases the MSLP in the region. This leads to a decrease in the MSLP contrast between the Orinoco and the Andes-Amazon transition region, and finally, a weakening of the flow associated with the OLLJ. The contrary occurs during strong OLLJ events: lower SSHF over the Orinoco relates to decreased NSAT in the region, increasing the MSLP locally and strengthening the MSLP gradient between the Orinoco and the Andes-Amazon transition region, therefore allowing the intensification of the OLLJ. In general, strong (weak) OLLJ events occurred during La Niña (El Niño), as also discussed by Builes-Jaramillo et al. (2022b), suggesting that the warm and cold phases of ENSO strongly influence the interannual strengthening of the OLLJ.

These results are consistent with Martinez et al. (2022) and confirm that although the meridional MSLP gradients between the Tropical North Atlantic and the Andes-Amazon transition are relevant for the development of the OLLJ, other regional aspects like the surface fluxes between the northern and southern zones of the OLLJ corridor affect the MSLP conditions in those regions, influencing the OLLJ strength during its activation period. It is important to notice that although the patterns of the gradients of MSLP, SSHF, and NSAT tend to be distinctive depending on the intensity of the OLLJ, they are not always similar during all the selected events. One example is 1982, when a strong El Niño occurred and a weak OLLJ event was identified but the patterns of decreasing MSLP and increasing air temperature and SSHF gradients are not very clear. Similarly, not all the changes in these gradients are related to a change in the OLLJ intensity. This suggests that gradients between the northern and southern regions of the OLLJ corridor influence the strengthening of the surface wind field but may not be the only elements to consider to evaluate a change in the intensity of the OLLJ, for which further studies are needed.

3.2 The OLLJ in CMIP6 models

3.2.1 Classification of the CMIP6 models

Initially, to identify if the main biases in the representation of the OLLJ arise from difficulties in the representation of a particular wind component, we compare how CMIP6 models represent the OLLJ index in the region C3.4 using the zonal and meridional wind components individually as well as the

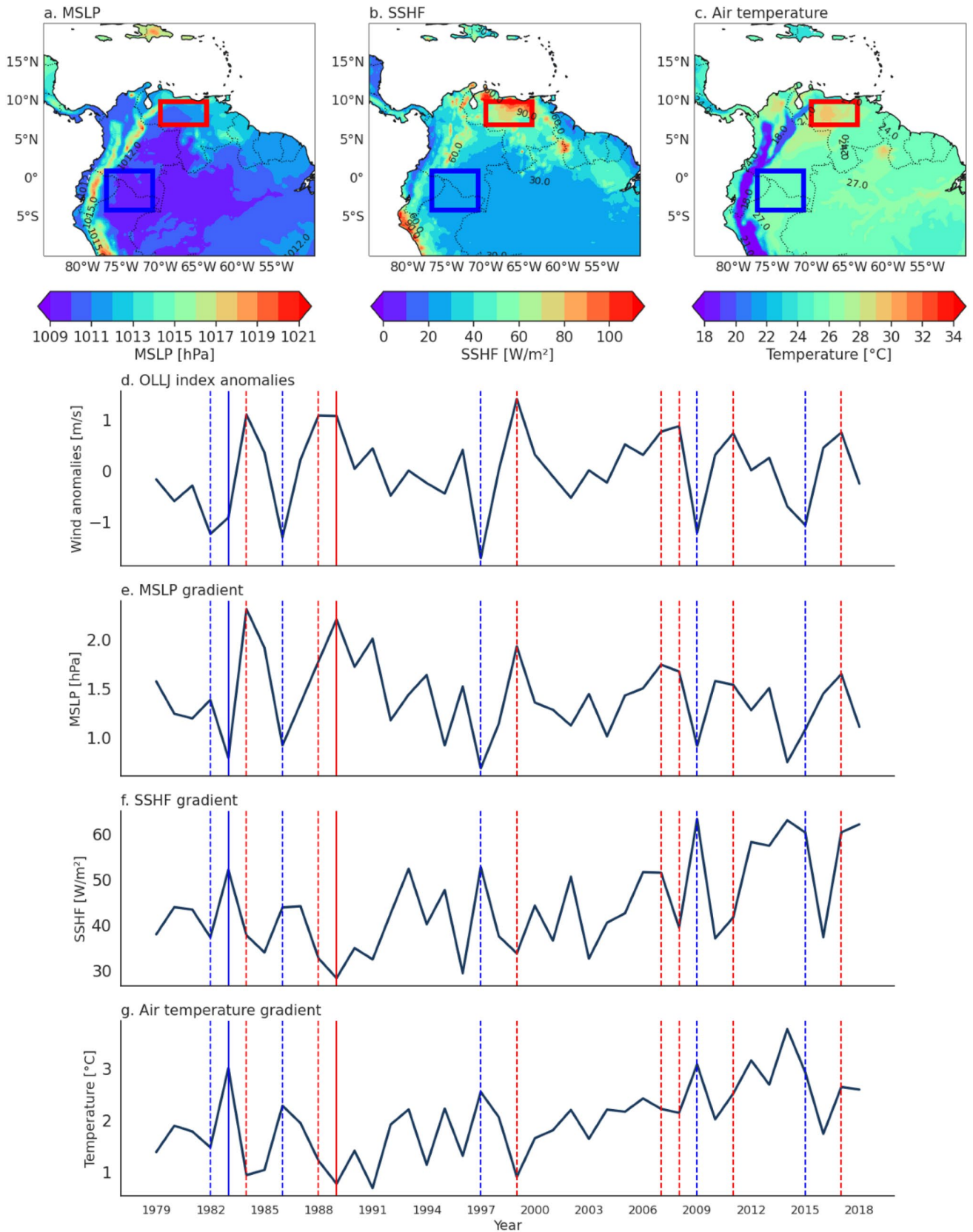


Fig. 3 Climatological **a** mean sea level pressure (MSLP), **b** surface sensible heat flux (SSHF), and **c** near-surface air temperature (NSAT) for December–January–February (DJF) estimated from ERA5 data during 1979–2019. **d** Anomalies of the OLLJ index at the region C3.4 for DJF using ERA5 data during 1979–2019. Gradients of **e** MSLP, **f** SSHF, and **g** NSAT between the Orinoco and the Andes–Amazon transition region. Red vertical lines indicate years with the occurrence of a strong OLLJ in DJF. Blue lines represent the years of occurrence of a weak OLLJ. Dashed lines indicate the occurrence of El Niño (blue) and La Niña (red) events

total wind magnitude. Figure 4 shows the multimodel mean of the annual cycle of the OLLJ index at the region C3.4 for the CMIP6 models during the historical period (1979–2014). The OLLJ index estimated using the zonal wind (orange line) exhibits smaller variations throughout the year, with little changes in the wind speed in DJF, which corresponds to the activation period of the jet, and JJA, which corresponds to its weakening period. In contrast, the OLLJ index from the meridional wind (blue line) displays marked changes during the year, allowing better identification of the strengthening and weakening periods of the jet. Moreover, the total wind magnitude (green line) loses some variability as the contrast between DJF and JJA decreases due to the pattern of both zonal and meridional wind components. Results from the standard error of the mean (SEM) between the OLLJ indices computed from ERA5 and the multimodal mean of CMIP6 models (error bars in Fig. 4) indicate that the estimations from zonal and wind magnitude exhibit significant differences from May to September, with values over 1 m/s, while these differences are smaller during the rest of the year. This is also observed for CMI5 models (Fig. S3). These variations are not obtained for the meridional wind, confirming the above-mentioned contrasts between ERA5 and the estimates from CMIP6 models when considering the zonal and wind magnitude for estimating the OLLJ index.

The estimates from CMIP6 models using the meridional wind show greater agreement with that obtained from ERA5 (black line), as both models and ERA5 exhibit contrasts of up to 7 m/s between DJF and JJA. On the contrary, the estimates of the models from zonal wind exhibit large differences with ERA5 since the models do not simulate marked variations of the index during the year. The above suggests that the considered GCMs tend to have difficulties simulating zonal wind in the region, and therefore the OLLJ index at the region C3.4 estimated from the wind magnitude may not show the best variation of the wind field at the jet exit. Hence, we estimate the OLLJ index from the spatial average

of the meridional wind component between 825 and 950 hPa in the region C3.4 for ERA5 and the CMIP6 models.

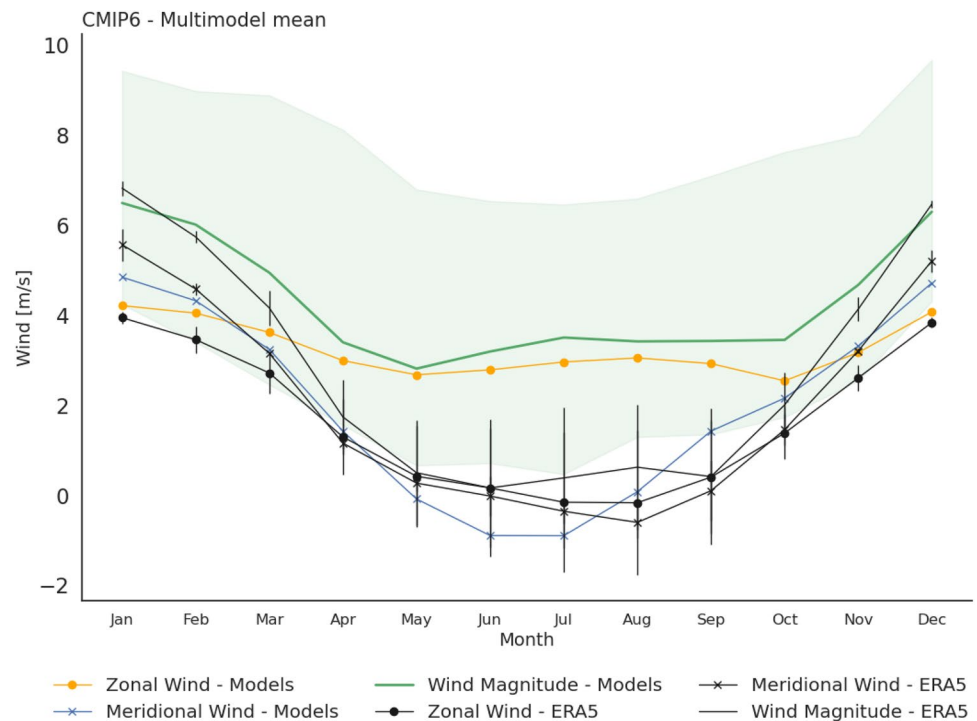
We classify the CMIP6 models in terms of their representation of the seasonal OLLJ characteristics, focusing on the RMSE and PCC estimates of the horizontal wind, vertical structure, and monthly OLLJ index. Based on these metrics, we perform a factor analysis to reduce the multicollinearity between these estimates and the number of observed variables to be considered in the cluster analysis. Figure 5a shows the scree plot of the factor analysis for the CMIP6 models. The scree plot indicates the number of factors to keep the largest amount of information of the original variables with the minimum number of factors. According to Fig. 5a, the number of factors to be retained from the CMIP6 estimates is three, retaining 91% of the original variance. The factors are the inputs for the cluster analysis based on Ward's minimum variance method (Ward 1963). At this point, to select the optimal number of clusters to be retained, we use the elbow method and the silhouette analysis (Rousseeuw 1987; Kodinariya and Makwana 2013; Figure S1), where the inflection point in the curve of the elbow plot can be related to an optimal number of clusters (Figure S1a). By contrast, the silhouette analysis considers that a set of k clusters in which not all clusters' silhouette coefficients are greater than the average (red line in Fig. S1) is not an adequate selection. At the same time, thicker silhouette plots may suggest the merge of different clusters into one, influencing the differentiation of specific clusters (Fig. S1b–g). Based on these criteria, we use $k=4$ clusters or groups.

Figure 5b shows the grouping of the CMIP6 models after performing the cluster analysis with the Ward's distance method shown in Fig. S1. Additionally, Fig. 5c shows the scatter plots of the three factors that represent 91% of the original variance. Table 1 shows the CMIP6 models included in each group. Following this classification, we evaluate how these GCMs represent the main characteristics of the OLLJ and its projected changes.

As previously discussed, the classification of the available CMIP6 models is based on two performance metrics (RMSE and PCC) for each season of the year; however, we focus on the DJF season as it corresponds to the activation period of the OLLJ.

The performance metrics of the CMIP6 clusters for the main characteristics of the OLLJ suggest that Groups 2 and 3 are the best among all clusters since they exhibit higher PCC and lower RMSE for all the characteristics analyzed here (Table 2). Note that clusters may have a high performance

Fig. 4 Multimodel mean of CMIP6 simulations of the OLLJ index in the region C3.4 during the historical period (1979–2014), as a function of zonal (orange line) and meridional (blue line) wind components, and the total wind magnitude (green line). The black line represents the OLLJ index using the ERA5 wind magnitude, while the green shading corresponds to the envelope of the model estimates of the OLLJ index using the total wind magnitude. The black lines with dots and crosses represent the OLLJ index estimated using zonal and meridional wind components from ERA5, respectively. Error bars correspond to the standard error of the mean between the series of ERA5 and the multimodel mean of the CMIP6 simulations



either in the spatial pattern or the error of the estimates of a particular characteristic but can have an inaccurate simulation of other OLLJ features. For instance, Groups 1 and 4 misrepresent the vertical structure of the jet (PCC of 0.52 and 0.56, respectively, and RMSE of 2.03 for both groups) but are more accurate in the simulation of the annual variation of the wind field at the jet exit region (PCC of 0.96 and 0.89, and RMSE of 0.66 and 0.99, respectively), supporting the importance of the analysis of different characteristics of this LLJ when analyzing GCMs. Most of the CMIP6 models considered in this work are able to simulate the temporal and spatial features of the OLLJ (Figure S2) and thus there is not much contrast among the performance of the four clusters obtained. However, according to the results of Table 2, we consider cluster 2 as the best group, while cluster 4 is taken as the worst group, with 6 and 8 models within each group, respectively.

The OLLJ climatological features simulated by GCMs were also evaluated with a set of 37 models included in the previous CMIP phase (CMIP5; Figure S3). We found that some CMIP5 models represent the temporal and spatial features of the low-level jet while others exhibit a poor performance. The above suggests an improvement in CMIP6 compared to CMIP5. CMIP6 models do not show significant contrasts among GCMs, as is the case of CMIP5 models,

with most of the models being able to simulate a low-level circulation over the Orinoco.

3.2.2 Simulation of the regional gradients of MSLP, NSAT and SSHF by the CMIP6 models

Previous studies state that the meridional pressure gradients between the NASH and the Intertropical Convergence Zone (ITCZ) modulate the strengthening of the northeastern trade winds and their southward shift, which in turn, enables the activation of the OLLJ (Builes-Jaramillo et al. 2022b; Martinez et al. 2022). Due to the role of these gradients in the jet activation, we assess their simulation by GCMs, as it allows us to relate variations in the representation of these patterns to the simulation of the OLLJ.

The climatology of MSLP and NSAT during DJF simulated by clusters (Fig. 6a, b, e, and f) show that the CMIP6 models capture the gradients of MSLP and NSAT between the tropical North Atlantic (orange rectangle) and the Andes-Amazon transition region (blue rectangle), with higher (lower) MSLP and lower (higher) NSAT over the tropical North Atlantic (Andes-Amazon transition region). These patterns are consistent with the strengthening of the wind field and its consequent direction into the continent. However, CMIP6 models, regardless of their simulation of the

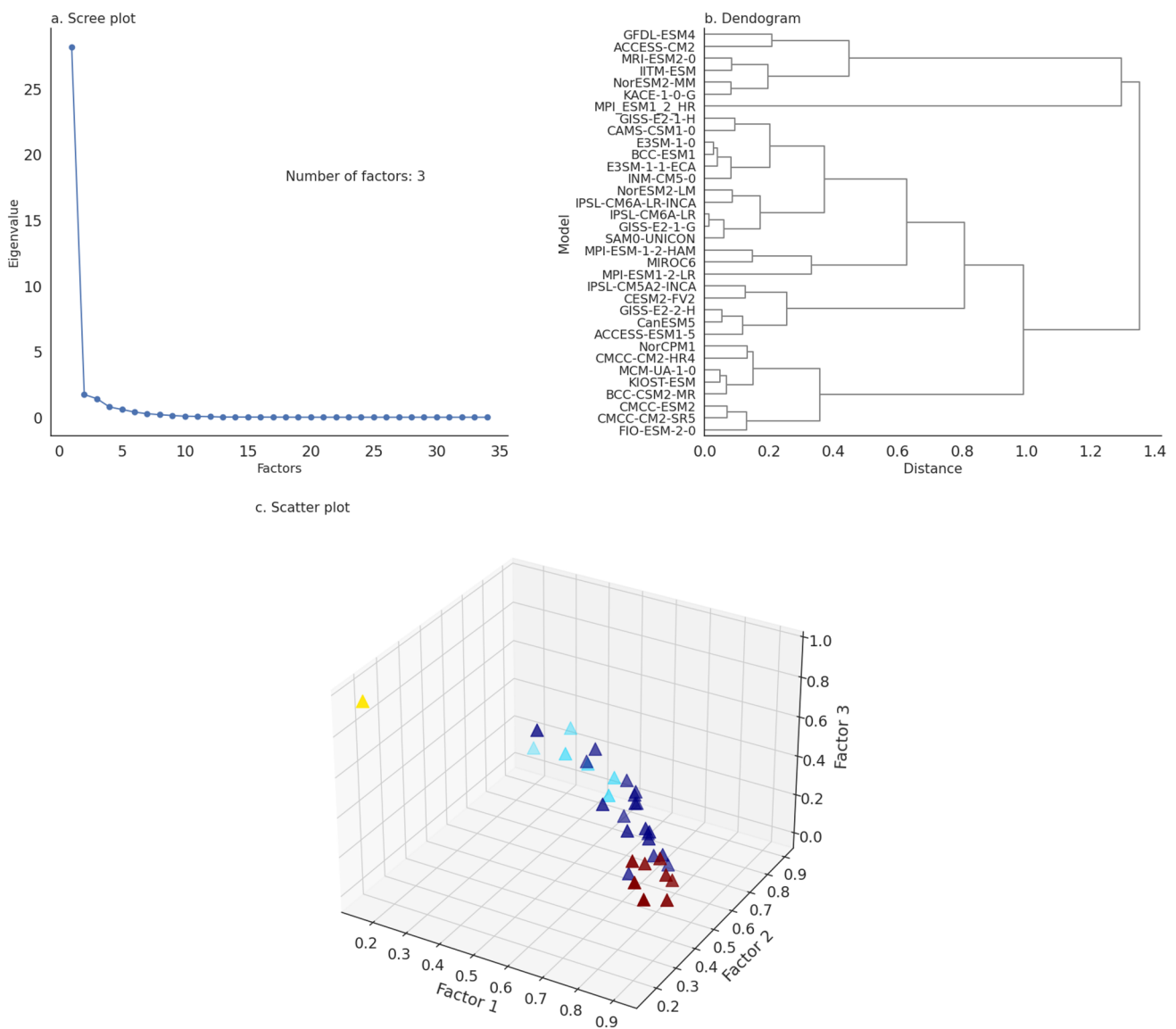


Fig. 5 **a** Scree plot of the factor analysis for the different metrics of the OLLJ main features from the CMIP6 models, **b** dendrogram of the cluster analysis, and **c** the scatter plot of the three factors considered

main OLLJ features, simulate a higher MSLP (lower NSAT) in the Atlantic than ERA5, while an opposite bias is obtained for the land mass (lower MSLP and higher NSAT; Fig. 6c, d, g, and h). These biases could produce an underestimation of the wind magnitude associated to the activation of the OLLJ by both groups of CMIP6 models (Figure S4). This suggests that in addition to these biases, which are shared among the clusters, other elements may modulate the differences in the performance of the models in their simulation of the wind field in northern South America.

On the other hand, Fig. 7a, b show the annual cycle of the historical simulation of the horizontal gradients of MSLP and NSAT between the Tropical North Atlantic and the Andes-Amazon transition region (orange and blue rectangles in Fig. 1, respectively). As discussed in Sect. 3.2.1, the CMIP6 clusters do not show marked differences in their performance in the simulation of the OLLJ. Similarly, the differences among clusters in the representation of the MSLP and NSAT gradients are not clear. Group 2 (best) has the highest correlation with ERA5 for both

Table 1 Classification of the CMIP6 models after the factor analysis and the cluster analysis

Group 1	Group 2	Group 3	Group 4
ACCESS-ESM1-5	ACCESS-CM2	MPI_ESM1_2_HR	BCC-CSM2-MR
BCC-ESM1	GFDL-ESM4		CMCC-CM2-HR4
CAMS-CSM1-0	IITM-ESM		CMCC-CM2-SR5
CanESM5	KACE-1-0-G		CMCC-ESM2
CESM2-FV2	MRI-ESM2-0		FIO-ESM-2-0
E3SM-1-0	NorESM2-MM		KIOST-ESM
E3SM-1-1-ECA			MCM-UA-1-0
GISS-E2-1-G			NorCPM1
GISS-E2-1-H			
GISS-E2-2-H			
INM-CM5-0			
IPSL-CM5A2-INCA			
IPSL-CM6A-LR			
IPSL-CM6A-LR-INCA			
MIROC6			
MPI-ESM-1-2-HAM			
MPI-ESM1-2-LR			
NorESM2-LM			
SAM0-UNICON			

gradients but it does not exhibit the lowest RMSE in all cases. On the other hand, Group 4 (worst) has the most prominent differences with ERA5 for the MSLP gradient (correlation of 0.88 and RMSE of 3.62) but improves its performance when simulating the NSAT gradient (correlation of 0.94 and RMSE of 0.96).

The multimodel mean and bias of the SSHF climatology (Fig. 6i–l) indicate that CMIP6 models simulate higher SSHF over northeastern South America and lower values of SSHF over the Andes-Amazon transition region. However, the CMIP6 models overestimate SSHF over the Orinoco.

Table 2 Performance metrics of the multimodel mean of the four clusters of the CMIP6 models considered, in terms of their simulation of the main characteristics of the Orinoco low-level jet

	Group 1	Group 2	Group 3	Group 4
Horizontal Wind PCC	0.88	0.92	0.91	0.88
Horizontal Wind RMSE	1.54	1.25	1.28	1.94
Vertical structure PCC	0.52	0.64	0.85	0.56
Vertical structure RMSE	2.03	1.77	1.13	2.03
OLLJ index PCC	0.96	0.98	0.97	0.89
OLLJ index RMSE	0.66	0.92	1.13	0.99

Metrics in bold correspond to the best value of the metric: higher PCC and lower RMSE

The biases of NSAT and SSHF do not show consistency in the Orinoco region, suggesting that NSAT biases can be more related to variations in MSLP or can be influenced by the ocean-landmass contrast. In turn, biases of SSHF can respond to other land-surface processes. As previously stated, the identified differences between the Orinoco and the Andes-Amazon transition region are strongly influenced by the climatological features of these regions: the Orinoco exhibits a drier climate that modulates a more arid regime over the region in comparison to the Andes-Amazon transition, which depicts a shift into a more humid regime.

We further analyze the simulation of the regional gradients of MSLP, NSAT, and SSHF between the entrance and exit regions of the OLLJ, and their links with the jet intensity. Figure 8 shows the composites of the anomalies of MSLP (panels a, b, g, and h), NSAT (panels c, d, i, and j), and SSHF (panels e, f, k, and l) during strong and weak OLLJ events for the best and worst groups of CMIP6 models (see Sect. 2.3). The composites are calculated considering the strong and weak OLLJ events during the DJF season, selected for each model from its long-term monthly anomalies of the OLLJ index. The results suggest that strong jet events (Fig. 8a, b, c, d, e, and f) are associated with higher MSLP and lower SSHF and NSAT over the Orinoco (larger regional gradients), while the opposite occurs during weak jet events (Fig. 8g, h, 8i, j, k, and l), for which the Orinoco region exhibits negative MSLP anomalies and positive NSAT and SSHF anomalies.

During strong OLLJ events, the anomalies of SSHF over the Andes-Amazon transition region (blue rectangle in

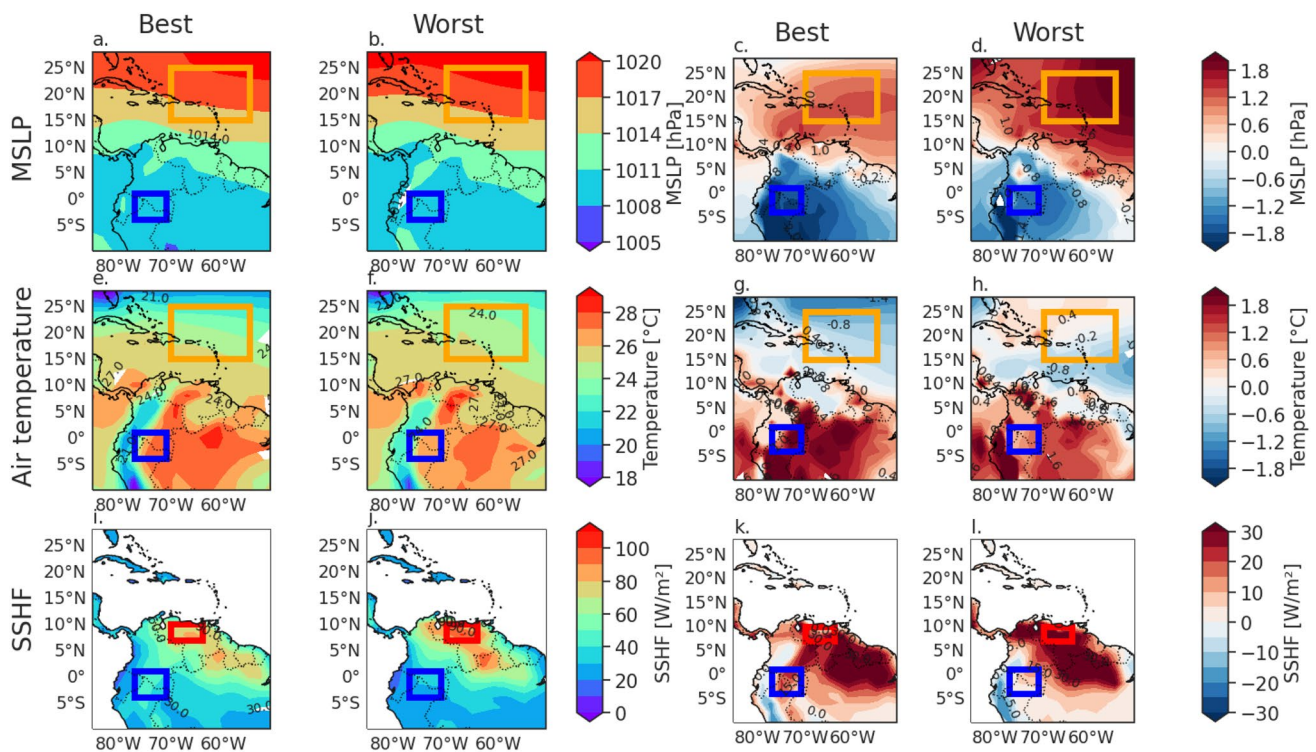


Fig. 6 Climatological **a, b** mean sea level pressure (MSLP), **e, f** near-surface air temperature (NSAT, and **i, j** surface sensible heat flux (SSHF) for December–January–February (DJF) from the CMIP6 models during 1979–2014. Mean bias of **c, d** MSLP, **g, h** NSAT, and

k, l SSHF. Rectangles represent the regions used to estimate the horizontal gradients: Tropical North Atlantic (orange), Orinoco (red), and Andes–Amazon transition (blue)

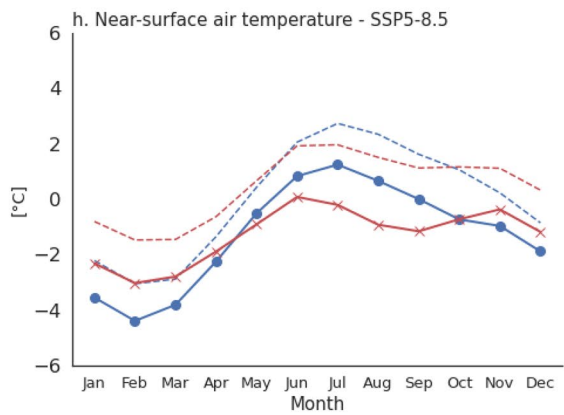
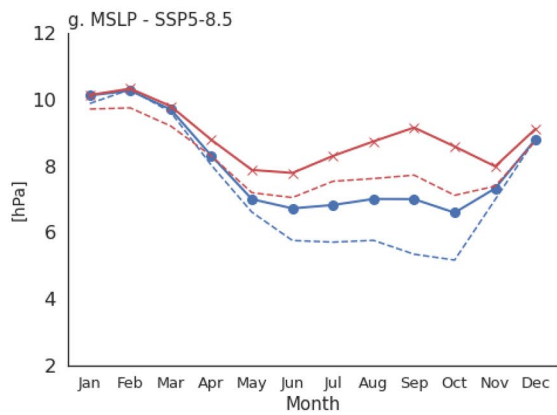
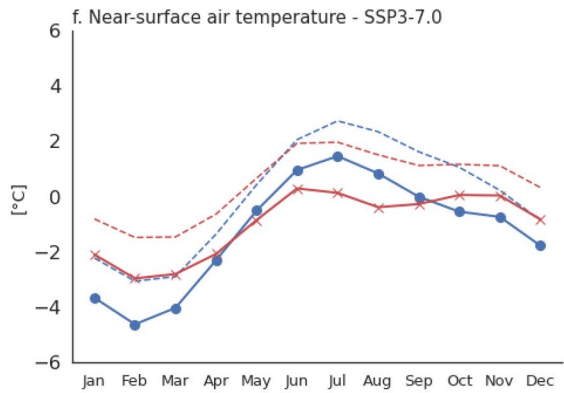
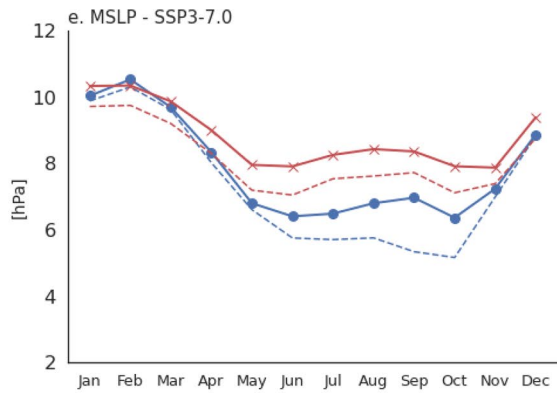
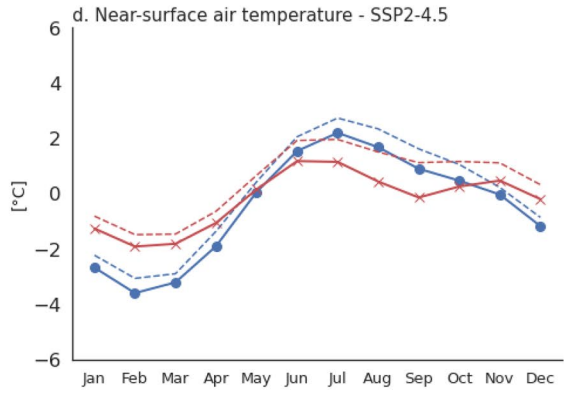
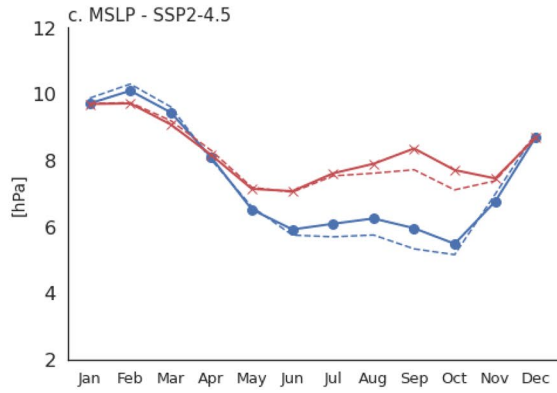
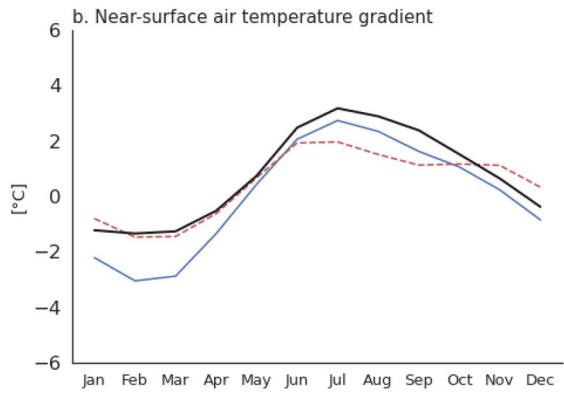
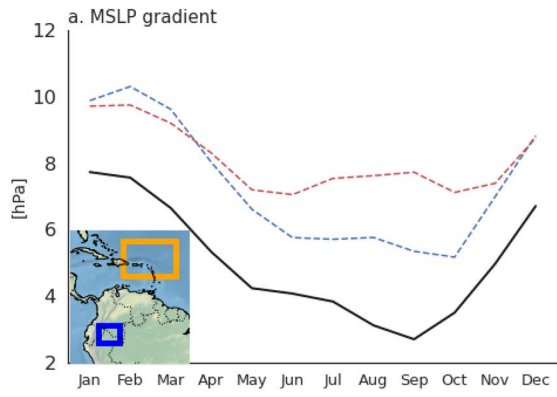
Fig. 8) are positive, suggesting that CMIP6 models simulate increases in the SSHF over the Andes–Amazon transition region alongside decreases over the Orinoco.

As identified in Fig. 8, interannual variations of the climatological conditions over the Orinoco region strongly influence the main features of the LLJ, as those variations modulate changes in the regional gradients between the northern and southern parts of the jet corridor. More generally, high SSHF over the Orinoco region increases NSAT, which in turn locally decreases the MSLP, weakening the regional MSLP gradient through the Orinoco basin and reducing the intensity of the OLLJ. On the contrary, decreasing SSHF in the Orinoco reduces NSAT while MSLP increases, strengthening the regional gradient, and therefore the low-level wind flow related to the OLLJ.

The estimates of the gradients of MSLP, NSAT and SSHF, defined as the difference between the mean values of the variable in the Orinoco minus the Andes–Amazon transition region during strong and weak OLLJ events, suggest the strengthening (weakening) of the gradient associated with

the occurrence of strong (weak) OLLJ events. During strong OLLJ events, the mean gradient of MSLP is 3.6 hPa, the gradient of NSAT is 0.88 °C, and the gradient of SSHF is 42.5 W/m². On the other hand, during weak OLLJ, the mean gradient of MSLP is 2.7 hPa, the gradient of NSAT is 1.7 °C, and the gradient of SSHF is 59.1 W/m². These estimates of the regional gradients are consistent with the patterns presented in Fig. 8: during strong events of the jet, the MSLP gradient is higher; in contrast, NSAT and SSHF gradients are lower (increased MSLP and decreased NSAT and SSHF over the Orinoco), while the opposite patterns occur during weak OLLJ events. It is relevant to clarify that during DJF, MSLP, NSAT, and SSHF values are higher over the Orinoco region (Fig. 6), and therefore gradients exhibit positive values but can vary depending on the contrasts between these regions.

The relationship between the OLLJ intensity and the fluctuations in the regional gradients is observed for all clusters of CMIP6 models, independently of their performance simulating the OLLJ main features. The above suggests the robustness of the relationship between the jet strengthening



--- Best - Historical --- Worst - Historical — ERA5 ● Best - projection × Worst - Projection

Fig. 7 Annual cycle of the gradients of mean sea level pressure (MSLP) and near-surface air temperature (NSAT) for **a, b** the historical experiment, and the projected changes for 2081–2100 (solid lines) under different scenarios: **c, d** SSP2-4.5, **e, f** SSP3-7.0, and **g, h** SSP5-8.5 for the best (blue line) and worst (red line) CMIP6 models, as well as ERA5 (black line). Dashed lines in **(c, d–h)** represent the mean annual cycle of the historical simulation (1979–2014) of each model cluster for comparative purposes

and the gradients of MSLP, SSHF, and NSAT between the Orinoco and the Andes-Amazon transition regions, which are strongly influenced by fluxes from the land surface, as proposed by Martinez et al. (2022).

Finally, to assess if the atmospheric circulation at mid levels of the troposphere is connected to the regional patterns at the surface and lower levels, Fig. 9a, b, e, and f present the multimodel mean fields of wind and specific humidity at 500 hPa during DJF for the best and worst CMIP6 clusters. During DJF, the wind field at 500 hPa is characterized by a strong easterly flow over northern Colombia, which is associated with the NASH, characterized by an anticyclonic pattern over the Caribbean Sea. The CMIP6 groups reproduce the anticyclone over the Caribbean Sea, although the strengthening of the wind pattern varies between groups.

Regarding the specific humidity at 500 hPa, models simulate greater values over the Amazon and smaller values over the Tropical North Atlantic Ocean, Caribbean Sea, and northern South America. These patterns are consistent with the southward location of the ITCZ and the occurrence of the South American Monsoon System (SAMS) during DJF when the higher values of specific humidity are expected to occur in the Amazon. On the other hand, models simulate drier conditions (reduced specific humidity) over northern South America and the tropical Atlantic, consistent with an anticyclonic circulation at the mid-troposphere. Even though the CMIP6 models capture the spatial patterns of specific humidity at mid-levels of the troposphere, the average bias of each cluster shows that models tend to underestimate the mid-tropospheric humidity in the tropical North Atlantic and northern South America (Fig. 9g, h), with the best group exhibiting the largest underestimation.

These results suggest that high values of SSHF and NSAT, which tend to be located over the Orinoco region (red rectangle in Fig. 6), are accompanied by a northeasterly flow and reduced specific humidity at mid levels, inducing drier conditions in the region. A different pattern occurs over the Andes-Amazon transition region (blue rectangle in Fig. 6), where wind circulation at 500 hPa is characterized by the convergence of northeasterly and easterly flows while the specific humidity increases, which can be related to more

humid conditions at the exit of the jet, as obtained by Segura et al. (2020) when analyzing rainfall in the Amazon. There does not seem to be a marked relationship between fluctuations in the simulated mid-level wind circulation and specific humidity and surface/low-level patterns, particularly for SSHF and NSAT (Fig. 6e, f, i, and j). This is based on the fact that the CMIP6 clusters tend to exhibit similar biases in the simulation of these features at 500 hPa while they do not show a clear signal on the surface and low-level patterns.

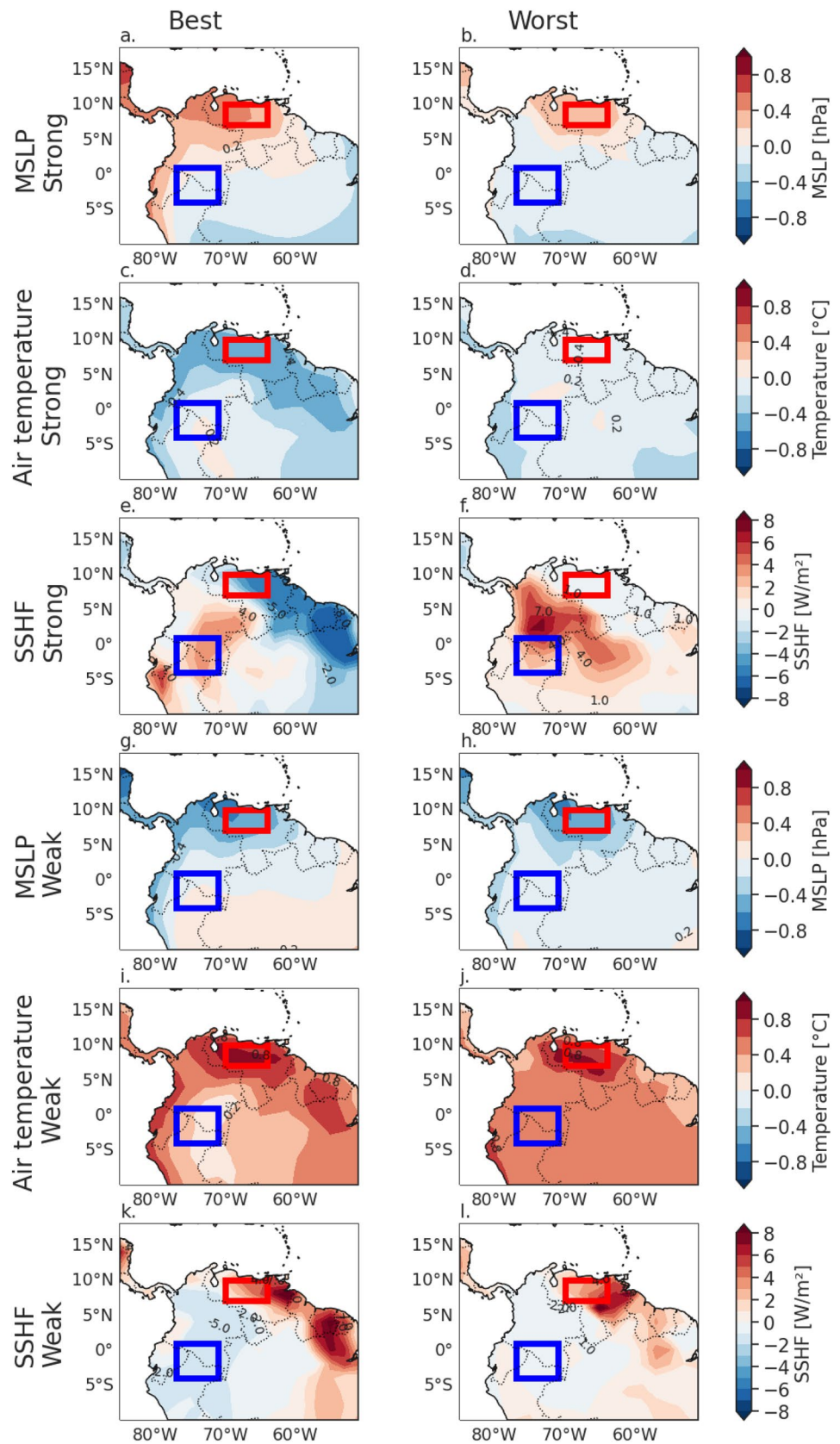
The VIMF between 800 and 1000 hPa simulated by the CMIP6 clusters for DJF (Fig. 9i and j) indicates smaller VIMF in western Colombia, Ecuador, and Peru, while the greatest values are located in the Caribbean Sea and northern Brazil. Some CMIP6 clusters properly simulate the VIMF in the Orinoco basin, with values of about 120 kg/ms. However, although a better simulation of the low-level VIMF can be related to a better simulation of the OLLJ, some biases may be added due to the misrepresentation of the specific humidity at lower pressure levels. The mean biases (Fig. 9k and l) suggest that models tend to underestimate the VIMF along the OLLJ corridor, and most of the CMIP6 clusters overestimate the low-level moisture flux in the western slope of the Los Andes mountain range and the northern Amazon.

3.2.3 Projected changes of the OLLJ

Figure 10 shows the projected changes of the wind field between 825 and 950 hPa during DJF from the groups with the best and worst simulation of the OLLJ main features for the long term (2081–2100) under different climate change scenarios. The groups exhibit negative projected changes, suggesting a weakening of the wind magnitude of the OLLJ by the end of the twenty-first century. In both groups, there is an agreement by most of the models in this projected weakening during DJF by the end of the twenty-first century, particularly at the exit of the OLLJ.

The slope of the projected changes of the OLLJ index during the twenty-first century is shown in Table 3. The trend analysis considers only the DJF season as it corresponds to the activation period of the OLLJ. Results indicate marked decreasing trends under all the considered SSPs and for all the groups of CMIP6 models with agreement among the model clusters, pointing to a weakening of this low-level circulation during the twenty-first century. This is consistently observed for all the scenarios, which suggests the robustness of the projections of the main characteristics of the OLLJ under different possible emission trajectories. Most of the CMIP6 clusters project a weakening of the OLLJ with a statistically significant trend, with a range of projected changes

Fig. 8 Composites of the anomalies of **a, b, g, h** mean sea level pressure (MSLP), **c, d, i, j** near-surface air temperature (NSAT), and **e, f, k, l** surface sensible heat flux (SSHG) in December–January–February (DJF) for the CMIP6 clusters during strong and weak Orinoco low-level jet events. Red and blue rectangles represent the Orinoco and the Andes–Amazon transition regions, respectively



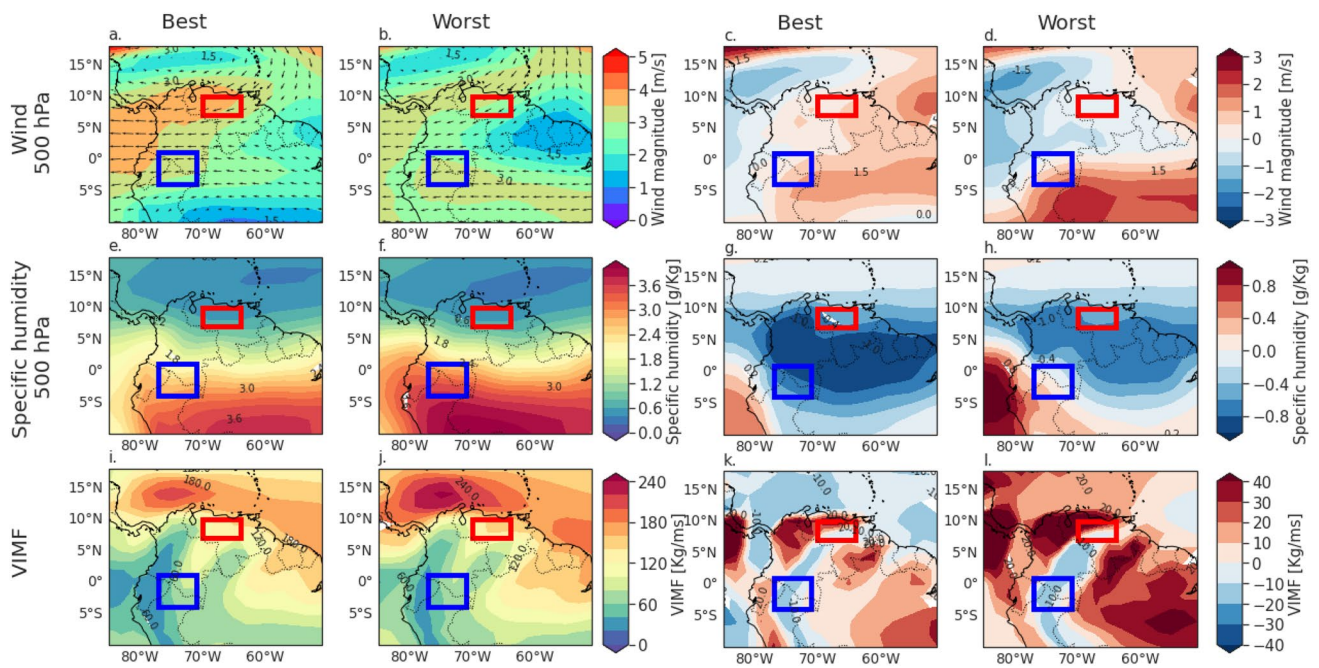


Fig. 9 Climatological **a, b** horizontal wind, **e, f** specific humidity, and **i, j** vertically integrated moisture flux (VIMF) between 800 and 1000 hPa for December–January–February (DJF) from CMIP6 models during 1979–2014. Mean bias of **c, d** horizontal wind, **g, h** spe-

cific humidity, and **k, l** VIMF between 800 and 1000 hPa. Red and blue rectangles represent the Orinoco and the Andes–Amazon transition regions, respectively

in meridional wind velocity of about 0.05 m/s per decade (from a reference meridional wind velocity of 4.6 m/s for DJF, according to the CMIP6 multi-model mean in the historical experiment).

Regarding the projections of the gradients of MSLP and NSAT between the ocean and the South American landmass, results suggest that there are no marked projected changes in the gradients of MSLP in CMIP6 during DJF by the end of the twenty-first century (Fig. 7c, e, and g), but the projected changes in the gradients of MSLP tend to be enhanced under climate scenarios with a higher radiative forcing (Fig. 7g). In addition, there is no agreement between the best and worst clusters, independently of the scenario considered, in terms of the projected variations of the MSLP gradients between the ocean and the northern South American landmass during DJF. This pattern is not shared for JJA, as results from the MSLP gradients exhibit high variations between the groups during those months. However, when considering the NSAT gradients (Fig. 7d, f, h), the projected changes of the temperature contrasts suggest marked variations with respect to the historical simulations during DJF. This is based on the fact that the CMIP6 clusters tend to exhibit lower NSAT

gradients during 2081–2100 (solid lines) with respect to the historical simulations (dashed lines), indicating greater contrasts between the ocean and the northern South American landmass. This is consistent with previous studies suggesting that increasing temperatures over land in northern South America are one of the most prominent projected changes in the region according to CMIP6 models (e.g. Reyer et al. 2017; Almazroui et al. 2021; Arias et al. 2021a, b).

The increasing contrasts of NSAT between the Tropical North Atlantic and the Andes–Amazon transition region could strengthen the wind circulation into the continent, which is not consistent with the projected weakening and shrinking of the OLLJ suggested by Fig. 10 and Table 3. This suggests that other processes aside from the thermal contrast between the ocean and the northern South American landmass may influence the projected changes of the OLLJ.

To assess this in more detail, the projected changes of MSLP, NSAT, and SSHF in northern South America, which are relevant to assess changes in the contrasts between the northern and southern regions in the OLLJ corridor, are shown in Fig. 11. The projected changes for both clusters in CMIP6 indicate decreasing MSLP through the OLLJ

Fig. 10 Projected changes of the DJF wind field between 825 and 950 hPa for the best and worst CMIP6 clusters, for the long term (2081–2100) under different scenarios: **a, b** SSP2-4.5, **c, d** SSP3-7.0, and **e, f** SSP5-8.5. Dots represent the grid cells with agreement in the sign of change of at least 80% of the models within each cluster

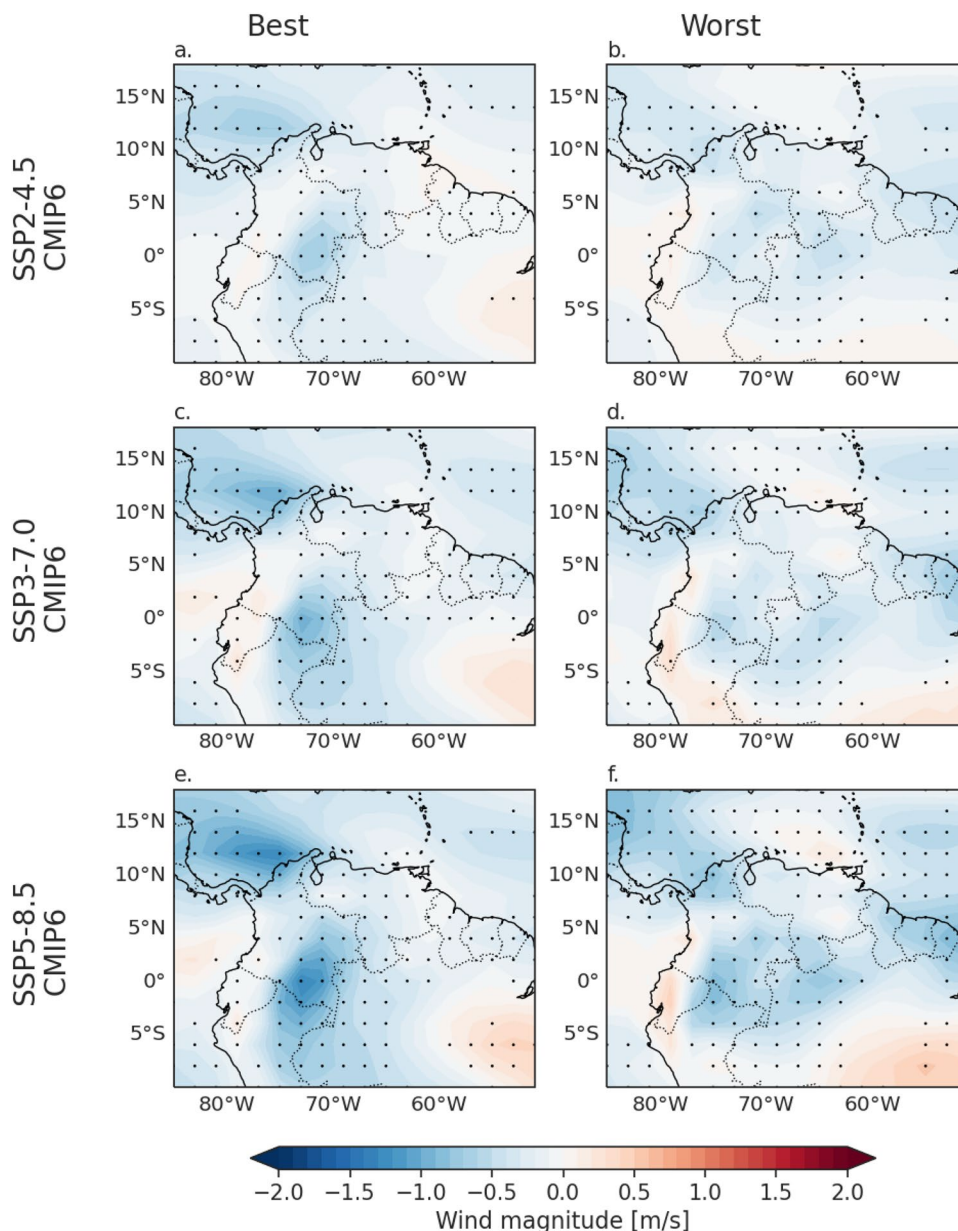


Table 3 Slope of the projected changes of the OLLJ index for DJF in m/s per decade

	Best	Worst
SSP2-4.5	-0.037	-0.052
SSP3-7.0	-0.039	-0.040
SSP5-8.5	-0.067	-0.058

All trends are statistically significant according to a Mann-Kendall test
 Negative values indicate decreasing trends

corridor (Fig. 11a–f) while increasing NSAT and SSHF (Fig. 11g–l, and m–r, respectively) are projected mainly over the Orinoco region (red rectangle). The pattern of increasing SSHF and NSAT over the Orinoco region tends to exhibit higher agreement among most of the models of the clusters (represented by dots in Fig. 11), which in turn may be related to the regional gradients that modulate the intensity of the OLLJ.

Projected changes of MSLP are not particularly confined to the Orinoco region in all CMIP6 clusters and scenarios. By contrast, projections of NSAT and SSHF show greater

positive changes over the Orinoco region (red rectangle in Fig. 11) in contrast to the Andes-Amazon region (blue rectangle in Fig. 11). The above suggests that the MSLP changes simulated by the CMIP6 models by the end of the twenty-first century mainly respond to variations in the projected warming across South America (e.g., Reboita et al. 2014; Llopart et al. 2020) although these models do not tend to adequately capture the signal of the regional gradients.

The variations in SSHF, especially over the Orinoco region, may explain the projected weakening of the OLLJ as increasing SSHF in the northern part of the jet corridor enhances the NSAT increase over that region and, consequently, the changes in the gradients between the northern and southern OLLJ corridor. It is relevant to highlight that the Andes-Amazon transition region is also expected to experience increases in NSAT and SSHF. Following Martinez et al. (2022), variations at the entrance of the jet can be more influential on the dynamics of the OLLJ; therefore, the increase in SSHF in the Orinoco region could modulate the projected weakening of the OLLJ. When comparing the projected changes under different scenarios, it is observed that higher radiative forcing induces greater changes in the regional patterns of MSLP, NSAT, and SSHF, the latter particularly over the Orinoco region. It is relevant to highlight that the contrasts between the Orinoco and the Andes-Amazonas region are more marked for SSHF, while the MSLP and NSAT patterns tend to be distributed in northern South America in response to the projected increase in continental temperatures. This may induce small contrasts between the northern and southern parts of the OLLJ corridor for MSLP and NSAT (Figure S5), reinforcing the relevance of changes in SSHF to OLLJ variations.

Focusing on the projected changes of the mid-level wind circulation under the different scenarios considered for the long term (2081–2100; Fig. 12a–f), projections suggest great contrasts between the CMIP6 clusters. The predominant pattern in the projected changes in wind magnitude at 500 hPa is the increase in wind speed over northeastern South America, northern Amazon, Ecuador, and northern Peru, and the decrease over the Caribbean Sea, northern Colombia, and northern Venezuela. The agreement among the models of the different groups is limited to a small region (the Caribbean sea, northern Brazil and Peru, Ecuador, and southern

Colombia). The above indicates that even though the projected patterns of wind magnitude at mid-levels exhibit great variability among models, the increase of the wind magnitude over northeastern South America and northern Amazon and the decrease over the Caribbean Sea are among the predominant patterns shared by most of the clusters under all scenarios.

In terms of the specific humidity at 500 hPa (Fig. 12g–l), the CMIP6 models agree on the increase of the mid-level specific humidity for 2081–2100 over most of the northern South American landmass, independently of the scenario. The pattern of projected increases of 500 hPa specific humidity exhibits high agreement among models under different radiative forcing conditions, indicating a common signal. These projections agree with previous studies that suggest the overall increase in specific humidity in the troposphere in a warming climate (e.g. Allan et al. 2020; Douville et al. 2021; Lee et al. 2021). The projected increase in mid-level specific humidity is stronger over the Amazon while it exhibits smaller changes over the Caribbean Sea.

The projected changes in the wind circulation and specific humidity at 500 hPa over northern South America, specifically the northern part of the OLLJ corridor, suggest increases in both wind magnitude and specific humidity at this level, although changes in the latter do not reach high values in comparison to the northern Amazon. Instead, although the specific humidity presents a projected increase at the entrance of the jet, values are close to zero. The effect of enhanced mid-level wind speeds over the Orinoco region and northeastern South America (red rectangle in Fig. 11) can lead to increased moisture drag out of the region, which in turn can induce drier conditions at the surface, as previously identified in the analysis of precipitation projections over the region (Zaninelli et al. 2019), thus enhancing the SSHF patterns over the Orinoco (Fig. 11m–r).

Similar to the projections of 500 hPa specific humidity, the projected changes of the VIMF in northern South America (Fig. 12m–r) suggest an increased 1000–800 hPa VIMF during DJF by the end of the twenty-first century in most of the northern South American domain. This pattern shows high agreement between the CMIP6 models over the Caribbean Sea and northeastern Brazil. However, one of the CMIP6 clusters projects reduced VIMF at the exit of the OLLJ (Fig. 12o),

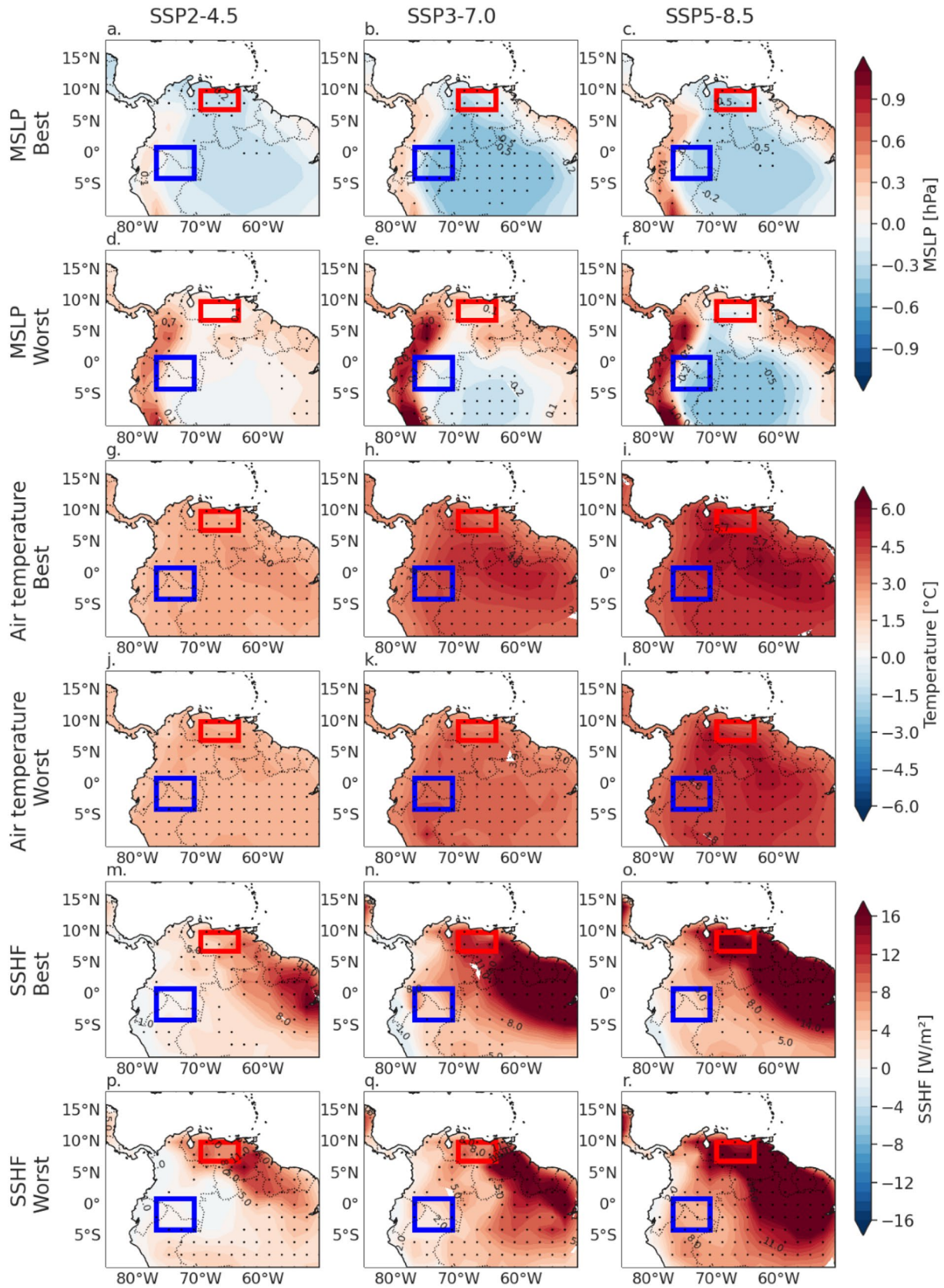


Fig. 11 Projected changes of the **a–f** mean sea level pressure (MSLP), near-surface air temperature (NSAT), and **m–r** surface sensible heat flux (SSHF) during December–January–February (DJF) for the long term (2081–2100) under different scenarios: **a, d, g, j, m, p** SSP2-4.5, **b, e, h, k, n, q** SSP3-7.0, and **c, f, i, l, o, r** SSP 5–8.5 for the best and worst CMIP6 clusters. Dots represent grid cells where there is an agreement of at least 80% of the models within each group in the sign of the projected change. Red and blue rectangles represent the Orinoco and the Andes–Amazon transition regions, respectively

which may be linked to the weakening of the low-level circulation along the Orinoco basin. These patterns through the jet corridor have a low agreement between the models of each cluster, suggesting uncertainties in the projected changes of low-level VIMF over the OLLJ region.

3.3 Links between the OLLJ and VIMF simulated by the CMIP6 models

As an additional assessment necessary to understand how CMIP6 models simulate the OLLJ and its links with atmospheric moisture transport in northern South America and their future projections, we perform a simple linear regression between the anomalies of the OLLJ index and the anomalies of the VIMF in each grid cell (Fig. 13). For this analysis, we focus on the VIMF between 825 and 950 hPa. Here, we show the regression patterns of the MPI-ESM1-2-HR model, which has a high mean PCC and a low mean RMSE in all the main features of the jet (i.e. it shows a better simulation of the low-level wind field in northern South America), and the KIOST-ESM model, which has a low PCC and a high RMSE (i.e. it has a more biased simulation of the low-level wind field in the region). The results from ERA5 (Fig. 13a) suggest a positive relationship between the OLLJ intensity and the VIMF along the OLLJ corridor, with negative relationships in limited regions over the Andes and Brazil. This analysis indicates that a strengthening of the OLLJ is associated with high VIMF in the Orinoco basin and northern Amazon (including the Andes–Amazon transition region), and low VIMF in northern Brazil (the opposite when the OLLJ is weak).

The models with a better performance simulating the main features of the OLLJ (Fig. 13b) capture the positive relationship between the intensity of the OLLJ and the VIMF in the Orinoco basin and the northern Amazon, as observed from ERA5. Also, the MPI-ESM1-2-HR model simulates the negative link between the OLLJ index and VIMF in northern Brazil and the Andes, as the reference database suggests. The model with the worst representation of the low-level wind circulation in northern South America also

tends to misrepresent the links between the OLLJ intensity and the atmospheric moisture flux in the region (Fig. 13c). The above suggests that CMIP6 models are able to capture the spatial linkages between the jet activity and the VIMF in northern South America; however, their performance in simulating this link seems to be strongly related to their ability to simulate the low-level wind circulation in the region.

Regarding the climate projections of the links between the activity of the OLLJ and the VIMF at lower pressure levels, we consider the projected changes under the SSP2-4.5 and SSP5-8.5 pathways. The SSP3-7.0 scenario was not included due to the lack of data availability for these particular models. Figure 13d–g show marked variations between the two models in the historical experiment. In both SSP2-4.5 and SSP5-8.5 scenarios, the OLLJ relationship between the VIMF and the OLLJ index in northern South America is positive over the Orinoco basin but negative in western South America and northern Amazon. For the KIOST-ESM model (Fig. 13e and g), the regression coefficients are not very well marked in the SSP4.5 scenario, while the model suggests a reduced linear relationship between the OLLJ and the VIMF under the SSP5-8.5 scenario. By contrast, the MPI-ESM1-2-HR model (Fig. 13d and f) does exhibit significant coefficients, suggesting positive values limited to northeastern South America and the Orinoco basin. However, in the long term, this pattern does not extend to Peru, as the historical simulation suggests.

A preliminary analysis of the links between the OLLJ activity and regional precipitation patterns, performed from ERA5 and a set of CMIP6 models with the best simulation of the features of the OLLJ (Figure S6), indicates that an enhanced OLLJ may decrease precipitation along the Orinoco basin and the northern Amazon (Figure S6a). This pattern is not completely simulated in the historical experiment by the CMIP6 models considered, which lose statistical significance at the exit of the jet (Figures S6b, S6d, S6f, and S6h). On the other hand, climate projections by the end of the twenty-first century (2081–2100; Figures S6c, S6e, S6g, and S6i) for the SSP3-7.0 scenario do not suggest significant changes with respect to the historical simulation, as negative regression coefficients are observed at the entrance of the jet, while the relationship tends to decrease at the exit of the jet and the northern Amazon. As widely known, GCMs exhibit limitations in their simulation of precipitation over the region, thus further analyses are needed to assess the response of regional precipitation patterns to the projected weakening of the OLLJ.

These results highlight the role of the OLLJ in atmospheric moisture patterns in northern South America, as the

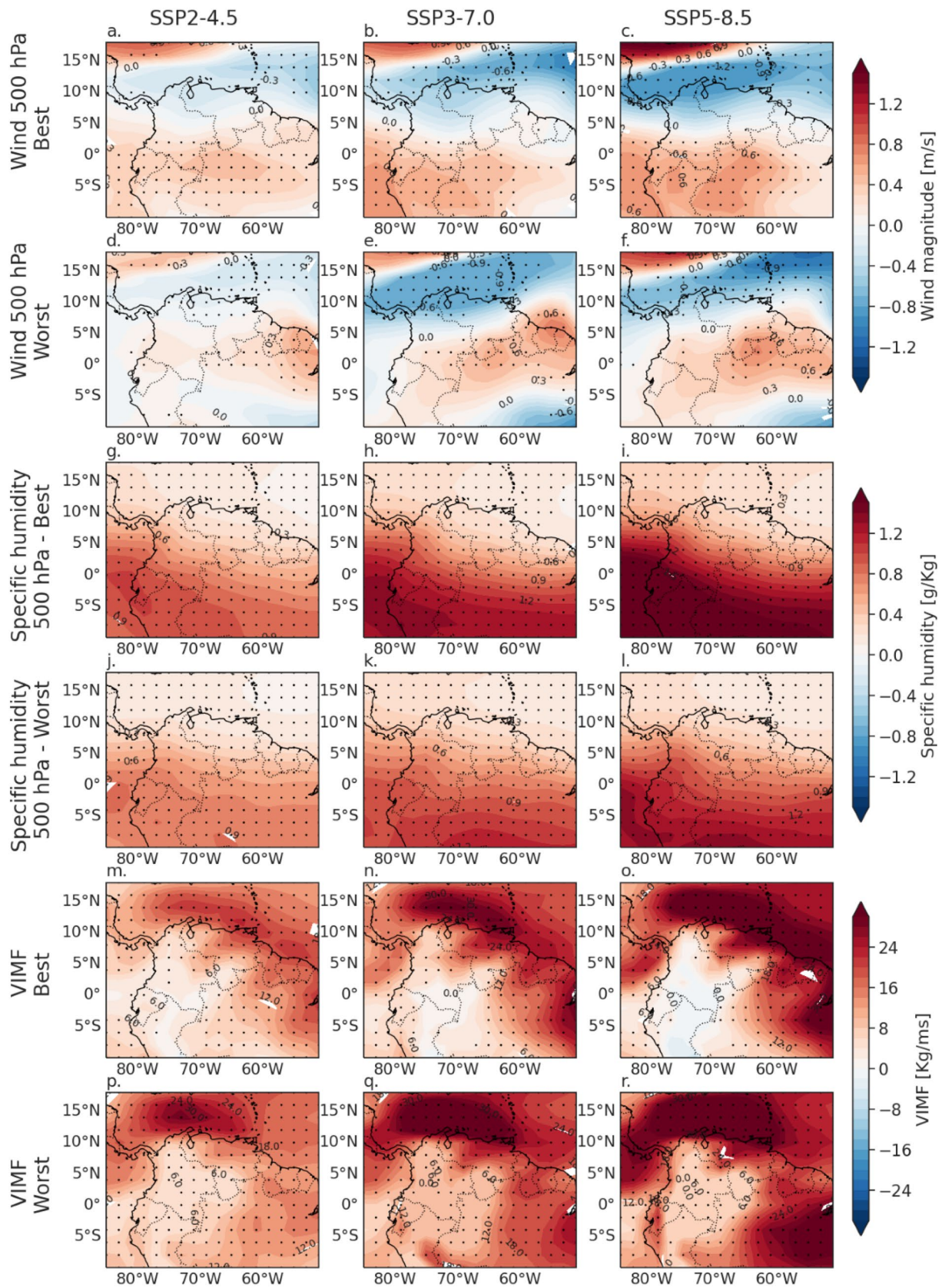


Fig. 12 Projected changes of the **a–f** 500 hPa horizontal wind, **g–l** 500 hPa specific humidity, and **m–r** 1000–800 hPa vertically integrated moisture flux (VIMF) during December–January–February (DJF) for the long term (2081–2100) under different scenarios: **a, d, g, j, m, p** SSP2-4.5, **b, e, h, k, n, q** SSP3-7.0, and **c, f, i, l, o, r** SSP 5–8.5 for the best and worst CMIP6 clusters. Dots represent grid cells where there is an agreement of at least 80% of the models within each group in the sign of the projected change

projected weakening of this jet under different scenarios induces variations in the low-level VIMF in northern South America. Specifically, regions with high VIMF due to higher wind speed at the exit of the jet are limited to the Orinoco basin and northeastern South America. This relationship is observed for the reference data (ERA5) (Fig. 13a) and the historical simulation of the CMIP6 models (Fig. 13b and c). However, projections no longer exhibit this link over the southernmost regions (Fig. 13d–g).

4 Summary and discussion

We analyzed the main features of the Orinoco low-level jet (OLLJ), the links with atmospheric moisture transport and moisture-related processes in northern South America, and the ability of models included in the sixth phase of the Coupled Model Intercomparison Project (CMIP6) to simulate these features in the historical experiment. Additionally, we focused on the twenty-first century projections of these aspects of the OLLJ under different emission scenarios.

We analyzed the information of 34 CMIP6 models and classified the set of models in terms of their seasonal simulation of the low-level wind circulation in northern South America. To do this we considered the Pattern Correlation Coefficient (PCC) and the Root Mean Square Error (RMSE) of the seasonal spatial patterns. The evaluation of the model performance was based on the horizontal wind between 825 and 950 hPa, a vertical cross-section across the jet corridor and the vertical structure of the wind field at the exit of the jet, and the monthly variations of the meridional wind using the OLLJ index proposed in this study. After obtaining the PCC and RMSE values of these estimates with respect to the ERA5 reanalysis, these metrics were used as the input for the factor analysis, and the resulting factors were, at the same time, the input to the cluster analysis (Fig. 5). This evaluation shows that the CMIP6 models tend to adequately simulate the spatial and temporal features of the OLLJ, exhibiting a similar performance among groups. Our analysis indicates that the performance of a set of 37 CMIP5 models tends to

exhibit higher contrasts among models (not shown), suggesting an improvement of CMIP6 over CMIP5 in simulating the OLLJ main features.

Following Martinez et al. (2022), we assessed how CMIP6 models link the interannual variations of the OLLJ intensity with the regional contrasts of mean sea level pressure (MSLP), near-surface air temperature (NSAT), and surface sensible heat flux (SSHF) between the Orinoco and the Andes-Amazon transition region (red and blue rectangle in Fig. 1). Our results indicate that CMIP6 models capture the regional variations associated with changes in the OLLJ interannual strengthening independently of their simulation of the main features of this circulation (Fig. 8). These findings show that the CMIP6 models can represent the low-level atmospheric circulation in northern South America, as they can associate fluctuations in the gradients between the northern and southern regions of the OLLJ corridor with changes in the intensity of the low-level wind in the Orinoco basin. Olmo et al. (2022) showed that some of the CMIP6 models are able to represent the low-level circulation over tropical South America, based on a weather pattern classification approach. This highlights that, although CMIP6 models still have large biases simulating variables like precipitation in the region (Almazroui et al. 2021; Arias et al. 2021b; Ortega et al. 2021), they may have a better representation of the dynamic process associated with precipitation, such as low-level circulations.

Finally, after analyzing the climate projections of the main OLLJ features, the most notable change of the OLLJ in the long term (2081–2100) is its weakening and shrinking, as projected changes indicate reduced wind speed by the end of the twenty-first century along the Orinoco basin, specifically at the jet exit (Fig. 10 and Table 3). This pattern is observed under all the scenarios considered. However, the projected changes are greater for scenarios with higher radiative forcing (SSP5-8.5).

The projected weakening of the OLLJ may be driven by changes in the regional gradients of MSLP, NSAT, and, mainly, SSHF between the Orinoco and the Andes-Amazon transition region, instead of the influence of meridional gradients at larger scales, between the Tropical North Atlantic and the Amazon (Sect. 3.2.3). Projected changes in the gradients between the Orinoco and the Andes-Amazon transition region are strongly modulated by increased SSHF over the Orinoco region, which modifies the regional horizontal gradients in the OLLJ corridor.

Additionally, a simple linear regression analysis indicates that under the projected changes of the OLLJ (a weakening),

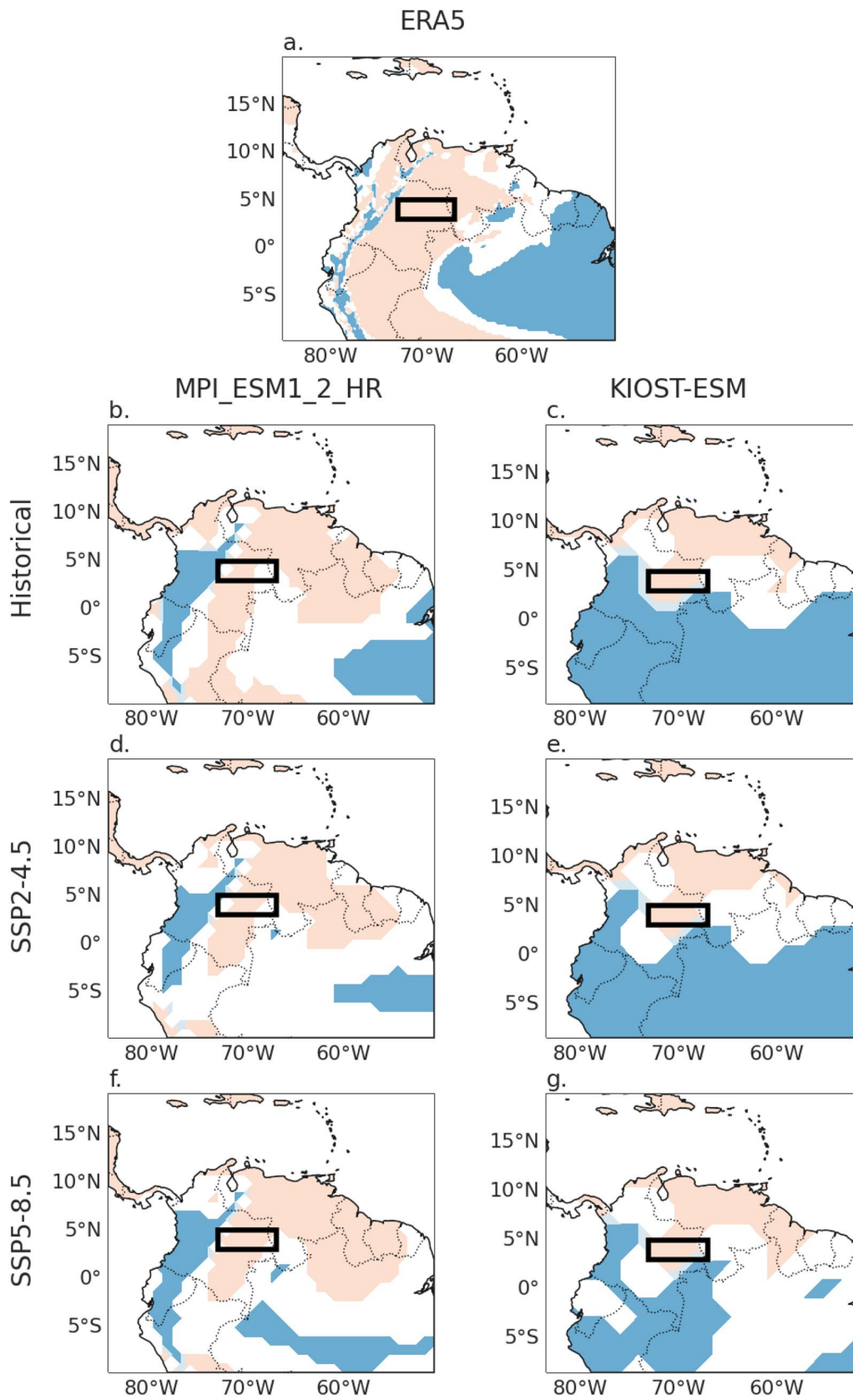


Fig. 13 Simple linear regression between the anomalies of the OLLJ index estimated in the region C3.4 (black rectangle) and the anomalies of VIMF in each grid cell using **a** ERA5, and two selected CMIP6 models (MPI-ESM1-2-HR and KIOST-ESM) for the **b, c** historical experiment and projections under the **d, e** SSP2-4.5 and **f, g** SSP5-8.5 scenarios. Colored cells represent a statistically significant relationship with an alpha of 0.05. Red (blue) colors represent a positive (negative) regression coefficient

its relationship with low-level VIMF in northern South America is also expected to vary (Fig. 13). In the historical period, the intensification of the low-level wind speed at the exit of the OLLJ enhances VIMF in northeastern South America and the Orinoco basin; however, this link is not observed across Peru in the climate projections, which indicates the shrinking of the region where the OLLJ enhances VIMF, thus representing major variations in atmospheric moisture patterns in the region.

These results acquire relevance in the context of the hydrological cycle intensification associated with anthropogenic climate change (e.g. Allan et al. 2020; Douville et al. 2021). The projected weakening of the OLLJ is expected to modulate variations on the hydroclimatological regimes in northern South America, such as those related to low-level moisture transport (Fig. 13). The variations in the moisture transport patterns can induce variations in the precipitation regimes, mainly at the exit of the jet, where the major changes in the VIMF are observed. Our preliminary results from precipitation do not suggest significant changes, as models fail to represent the links between the OLLJ and precipitation in northern South America (Figure S6). However, other studies have analyzed the changes in the precipitation and atmospheric moisture recycling and transport patterns over northern South America under future climate change scenarios (Arias et al. 2023), indicating a general increase in precipitable water while the response in precipitation is heterogeneous along the landmass, suggesting the importance of land-surface processes. Moreover, land cover changes over the Amazon, particularly the Andes–Amazon transition region, also modify atmospheric moisture transport over the region (e.g. Agudelo et al. 2019; Ruiz-Vásquez et al. 2020) as well as surface fluxes that could affect the OLLJ (e.g. Sierra et al. 2021b, 2023).

Figure 14a shows a general schematic of the main climatological features of the low and mid-level circulation in northern South America in association with the OLLJ. The activation of the OLLJ occurs due to the meridional gradients between the Tropical North Atlantic and the South American landmass, with high pressure over the ocean and low pressure over the land. These gradients enhance the

northeasterly trade winds circulation into the Orinoco basin, which contributes to the strengthening of the OLLJ during December–January–February (DJF) (Fig. 14a), when the jet exhibits its peak activity. The activation of the OLLJ occurs alongside local higher sensible heat flux from the surface (SSHF) in the northern part of the jet corridor due to the drier conditions over this region, where regional variations of the SSHF spatial distribution, alongside changes in NSAT and MSLP, modulate the interannual intensity of the OLLJ.

Regarding the projected changes of the OLLJ (Fig. 14b), the main projected variation is the weakening of the OLLJ during DJF, especially at its exit region, which in turn suggests a shrinking of the LLJ in its spatial domain. This change is expected to occur due to increasing SSHF over the northern part of the jet corridor (northeastern South America) as a consequence of stronger wind circulation at mid-levels (500 hPa) that increases moisture transport out of the region, enhancing drier conditions at the surface. On the other hand, projections of the meridional gradient between the Tropical North Atlantic and the South American landmass suggest its strengthening by the end of the twenty-first century, which would initially imply a strengthening of the OLLJ instead of a weakening. Therefore the projected weakening of the OLLJ may be more influenced by regional variations along the jet corridor than by ocean-landmass contrasts.

According to our results, the linkage between mid-level atmospheric moisture transport and near-surface conditions can influence the enhancement of future drier conditions in the Orinoco basin. The projected changes in wind circulation and specific humidity at 500 hPa over the Orinoco region during the activation period of the OLLJ (DJF) indicate that models project enhanced mid-level wind speed and specific humidity in northeastern South America by the end of the twenty-first century, which means stronger wind circulation that can drag the moisture out of the region, inducing drier conditions (Fig. 12). These results are consistent with previous studies focusing on projected changes in precipitation in South America, suggesting decreased precipitation in the Orinoco basin (Almazroui et al. 2021; Ortega et al. 2021). The projection of drier conditions over the Orinoco region is also suggested by the most recent report of the Intergovernmental Panel on Climate Change, which shows increased consecutive dry days as well as more frequent and intense agricultural and ecological droughts over this region (Arias et al. 2021a; Seneviratne et al. 2021). This is particularly important since the Orinoco and the Guiana Shield are very important regions in terms of biodiversity in South America (Bovolenta et al. 2018; Castellanos et al. 2022). This suggests

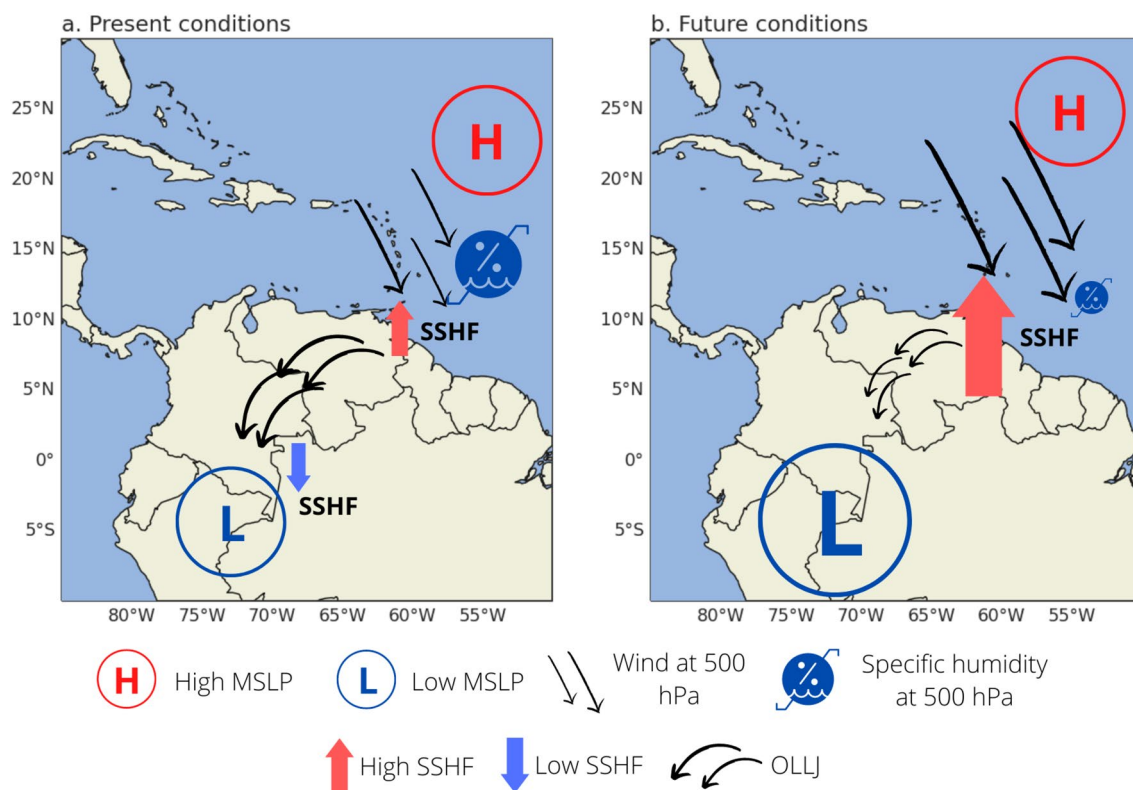


Fig. 14 General schematics of the **a** main climatological features during the historical period and **b** projected changes by the end of the twenty-first century under different emission scenarios for the low and mid-level circulation in northern South America during DJF, in

association with the OLLJ. Large (small) arrows and symbols indicate an increase (decrease) in each particular feature under future conditions

the importance of addressing research focused on this region given it is one of the most understudied regions in South America.

Supplementary Information The online version contains supplementary material available at <https://doi.org/10.1007/s00382-023-07028-7>.

Acknowledgements This work was funded by MINCIENCIAS through program No. 80740-490-2020 and by MINCIENCIAS grant 80740-238-2021.

Funding Open Access funding provided by Colombia Consortium.

Data availability ERA5 information is available in <https://cds.climate.copernicus.eu/cdsapp#!home>, while CMIP5/CMIP6 data is available in <https://esgf-node.llnl.gov/projects/esgf-llnl/>.

Declarations

Conflict of interest The authors declare no conflicts of interest.

Open Access This article is licensed under a Creative Commons Attribution 4.0 International License, which permits use, sharing, adaptation, distribution and reproduction in any medium or format, as long as you give appropriate credit to the original author(s) and the source, provide a link to the Creative Commons licence, and indicate if changes

were made. The images or other third party material in this article are included in the article's Creative Commons licence, unless indicated otherwise in a credit line to the material. If material is not included in the article's Creative Commons licence and your intended use is not permitted by statutory regulation or exceeds the permitted use, you will need to obtain permission directly from the copyright holder. To view a copy of this licence, visit <http://creativecommons.org/licenses/by/4.0/>.

References

- Acosta RP, Huber M (2017) The neglected Indo-Gangetic Plains low-level jet and its importance for moisture transport and precipitation during the peak summer monsoon. *Geophys Res Lett* 44(16):8601–8610. <https://doi.org/10.1002/2017GL074440>
- Agudelo J, Arias PA, Vieira SC, Martínez JA (2019) Influence of longer dry seasons in the Southern Amazon on patterns of water vapor transport over northern South America and the Caribbean. *Clim Dyn* 52:2647–2665. <https://doi.org/10.1007/s00382-018-4285-1>
- Albergel C, Dutra E, Munier S, Calvet JC, Muñoz-Sabater J, de Rosnay P, Balsamo G (2018) ERA-5 and ERA-Interim driven ISBA land surface model simulations: which one performs better? *Hydrol Earth Syst Sci* 22(6):3515–3532. <https://doi.org/10.5194/hess-22-3515-2018>
- Algarra I, Eiras-Barca J, Nieto R, Gimeno L (2019) Global climatology of nocturnal low-level jets and associated moisture sources

- and sinks. *Atmos Res* 229:39–59. <https://doi.org/10.1016/j.atmosres.2019.06.016>
- Al-Ghussain L (2019) Global warming: Review on driving forces and mitigation. *Environ Prog Sustain Energy* 38(1):13–21. <https://doi.org/10.1002/ep.13041>
- Allan RP, Barlow M, Byrne MP, Cherchi A, Douville H, Fowler HJ et al (2020) Advances in understanding large-scale responses of the water cycle to climate change. *Ann N Y Acad Sci* 1472(1):49–75. <https://doi.org/10.1111/nyas.14337>
- Almazroui M, Ashfaq M, Islam MN, Rashid IU, Kamil S, Abid MA et al (2021) Assessment of CMIP6 performance and projected temperature and precipitation changes over South America. *Earth Syst Environ* 5(2):155–183. <https://doi.org/10.1007/s41748-021-00233-6>
- Amador JA (1998) A climatic feature of the tropical Americas: the trade wind easterly jet. *Top Meteor Oceanogr* 5:91–102
- Amador JA (2008) The intra-Americas sea low-level jet: overview and future research. *Ann N Y Acad Sci* 1146(1):153–188. <https://doi.org/10.1196/annals.1446.012>
- Arias PA, Martínez JA, Vieira SC (2015) Moisture sources to the 2010–2012 anomalous wet season in northern South America. *Clim Dyn* 45:2861–2884. <https://doi.org/10.1007/s00382-015-2511-7>
- Arias PA, Martínez JA, Mejía JD, Pazos MJ, Espinoza JC, Wongchuig-Correa S (2020) Changes in normalized difference vegetation index in the Orinoco and Amazon River Basins: links to tropical Atlantic surface temperatures. *J Clim* 33(19):8537–8559. <https://doi.org/10.1175/JCLI-D-19-0696.1>
- Arias P, Bellouin N, Coppola E, Jones R, Krinner G, Marotzke J et al (2021a) Climate change 2021: the physical science basis. Contribution of Working Group I to the Sixth Assessment Report of the Intergovernmental Panel on Climate Change; Technical Summary. <https://doi.org/10.1017/9781009157896.002>
- Arias PA, Garreaud R, Poveda G, Espinoza JC, Molina-Carpio J, Masiokas M et al (2021b) Hydroclimate of the Andes Part II: hydroclimate variability and sub-continental patterns. *Front Earth Sci* 8:666. <https://doi.org/10.3389/feart.2020.505467>
- Arias PA, Ortega G, Villegas LD, Martínez JA (2021c) Colombian climatology in CMIP5/CMIP6 models: Persistent biases and improvements. *Revista Facultad De Ingeniería Universidad De Antioquia*. <https://doi.org/10.17533/udea.redin.20210525>
- Arias PA, Rendón ML, Martínez JA, Allan RP (2023) Changes in atmospheric moisture transport over tropical South America: an analysis under a climate change scenario. *Clim Dyn*. <https://doi.org/10.1007/s00382-023-06833-4>
- Balmaceda-Huarte R, Olmo ME, Bettoli ML, Poggi MM (2021) Evaluation of multiple reanalyses in reproducing the spatio-temporal variability of temperature and precipitation indices over southern South America. *Int J Climatol* 41(12):5572–5595. <https://doi.org/10.1002/joc.7142>
- Bao Y, Song Z, Qiao F (2020) FIO-ESM version 2.0: model description and evaluation. *J Geophys Res Oceans* 125(6):e2019JC016036. <https://doi.org/10.1029/2019JC016036>
- Barichivich J, Gloor E, Peylin P, Brienen RJ, Schöngart J, Espinoza JC, Pattanayak KC (2018) Recent intensification of Amazon flooding extremes driven by strengthened Walker circulation. *Sci Adv* 4(9):eaat8785. <https://doi.org/10.1126/sciadv.aat8785>
- Bonner WD (1968) Climatology of the low-level jet. *Mon Weather Rev* 96(12):833–850. [https://doi.org/10.1175/1520-0493\(1968\)096%3c0833:COTLLJ%3e2.0.CO;2](https://doi.org/10.1175/1520-0493(1968)096%3c0833:COTLLJ%3e2.0.CO;2)
- Boucher O, Servonnat J, Albright AL, Aumont O, Balkanski Y, Bastrikov V et al (2020) Presentation and evaluation of the IPSL-CM6A-LR climate model. *J Adv Model Earth Syst* 12(7):e2019MS002010. <https://doi.org/10.1029/2019MS002010>
- Bovolo CI, Wagner T, Parkin G, Hein-Griggs D, Pereira R, Jones R (2018) The Guiana Shield rainforests—overlooked guardians of South American climate. *Environ Res Lett* 13(7):074029. <https://doi.org/10.1088/1748-9326/aacf60>
- Builes-Jaramillo A, Yepes J, Salas HD (2022a) The Orinoco Low-Level Jet and its association with the hydroclimatology of northern South America. *J Hydrometeorol* 23(2):209–223. <https://doi.org/10.1175/JHM-D-21-0073.1>
- Builes-Jaramillo A, Yepes J, Salas HD (2022b) The Orinoco low-level jet during El Niño-Southern Oscillation. In *J Climatol*. <https://doi.org/10.1002/joc.7681>
- Burrows SM, Maltrud M, Yang X, Zhu Q, Jeffery N, Shi X et al (2020) The DOE E3SM v1.1 biogeochemistry configuration: description and simulated ecosystem-climate responses to historical changes in forcing. *J Adv Model Earth Syst* 12(9):e2019MS001766. <https://doi.org/10.1029/2019MS001766>
- Castellanos E, Lemos MF, Astigarraga L, Chacón N, Cuvi N, Huggel C, Miranda L, Moncassim Vale M, Ometto JP, Peri PL, Postigo JC, Ramajo L, Roco L, Rusticucci M (2022) Central and South America. In: Pörtner H-O, Roberts DC, Tignor M, Poloczanska ES, Mintenbeck K, Alegría A, Craig M, Langsdorf S, Löschke S, Möller V, Okem A, Rama B (eds) *Climate change 2022: impacts, adaptation and vulnerability. Contribution of Working Group II to the Sixth Assessment Report of the Intergovernmental Panel on Climate Change*. Cambridge University Press, Cambridge, pp 1689–1816. <https://doi.org/10.1017/9781009325844.014>
- Chai R, Mao J, Chen H, Wang Y, Shi X, Jin M et al (2021) Human-caused long-term changes in global aridity. *Npj Clim Atmos Sci* 4(1):1–8. <https://doi.org/10.1038/s41612-021-00223-5>
- Cherchi A, Fogli PG, Lovato T, Peano D, Iovino D, Gualdi S et al (2019) Global mean climate and main patterns of variability in the CMCC-CM2 coupled model. *J Adv Model Earth Syst* 11(1):185–209. <https://doi.org/10.1029/2018MS001369>
- Cook KH, Vizy EK (2010) Hydrodynamics of the Caribbean low-level jet and its relationship to precipitation. *J Clim* 23(6):1477–1494. <https://doi.org/10.1175/2009JCLI3210.1>
- Danabasoglu G (2019) NCAR CESM2-FV2 model output prepared for CMIP6 CMIP historical Versio Version 20191120. Earth System Grid Fed. <https://doi.org/10.22033/ESGF/CMIP6.11297>
- Douville H, Raghavan K, Renwick J, Allan RP, Arias PA, Barlow M, Cerezo-Mota R, Cherchi A, Gan TY, Gergis J, Jiang D, Khan A, Pokam Mba W, Rosenfeld D, Tierney J, Zolina O (2021) Water cycle changes. In: Masson-Delmotte V, Zhai P, Pirani A, Connors SL, Péan C, Berger S, Caud N, Chen Y, Goldfarb L, Gomis MI, Huang M, Leitzell K, Lonnoy E, Matthews JBR, Maycock TK, Waterfield T, Yelekçi O, Yu R, Zhou B (eds) *Climate change 2021: the physical science basis. Contribution of Working Group I to the Sixth Assessment Report of the Intergovernmental Panel on Climate Change*. Cambridge University Press, Cambridge, pp 1055–1210. <https://doi.org/10.1017/9781009157896.010>
- Dunne JP, Horowitz LW, Adcroft AJ, Ginoux P, Held IM, John JG et al (2020) The GFDL Earth System Model version 41 (GFDL-ESM41): overall coupled model description and simulation characteristics. *J Adv Model Earth Syst* 12(11):e2019MS002015. <https://doi.org/10.1029/2019MS002015>
- Espinoza JC, Garreaud R, Poveda G, Arias PA, Molina-Carpio J, Masiokas M et al (2020) Hydroclimate of the Andes Part I: main climatic features. *Front Earth Sci*. <https://doi.org/10.3389/feart.2020.00064>
- Eyring V, Bony S, Meehl GA, Senior CA, Stevens B, Stouffer RJ, Taylor KE (2016) Overview of the Coupled Model Intercomparison Project Phase 6 (CMIP6) experimental design and organization. *Geosci Model Dev* 9(5):1937–1958. <https://doi.org/10.5194/gmd-9-1937-2016>
- Gallego D, García-Herrera R, Gómez-Delgado FDP, Ordoñez-Perez P, Ribera P (2019) Tracking the moisture transport from the Pacific

- towards Central and northern South America since the late 19th century. *Earth Syst Dyn* 10(2):319–331. <https://doi.org/10.5194/esd-10-319-2019>
- Gimeno L, Stohl A, Trigo RM, Dominguez F, Yoshimura K, Yu L et al (2012) Oceanic and terrestrial sources of continental precipitation. *Rev Geophys*. <https://doi.org/10.1029/2012RG000389>
- Gimeno L, Dominguez F, Nieto R, Trigo R, Drumond A, Reason CJ et al (2016) Major mechanisms of atmospheric moisture transport and their role in extreme precipitation events. *Annu Rev Environ Resour* 41:117–141. <https://doi.org/10.1146/annurev-envir-on-110615-085558>
- Gimeno L, Vázquez M, Eiras-Barca J, Sorí R, Stojanovic M, Algarra I et al (2020) Recent progress on the sources of continental precipitation as revealed by moisture transport analysis. *Earth Sci Rev* 201:103070. <https://doi.org/10.1016/j.earscirev.2019.103070>
- Gimeno-Sotelo L, Gimeno L (2023) Where does the link between atmospheric moisture transport and extreme precipitation matter? *Weather Clim Extremes* 39:100536. <https://doi.org/10.1016/j.wace.2022.100536>
- Gimeno-Sotelo L, de Zea Bermudez P, Algarra I, Gimeno L (2022) Modelling hydrometeorological extremes associated to the moisture transport driven by the Great Plains low-level jet. *Stoch Env Res Risk Assess* 36(7):1917–1941. <https://doi.org/10.1007/s00477-022-02199-x>
- Golaz JC, Caldwell PM, Van Roekel LP, Petersen MR, Tang Q, Wolfe JD et al (2019) The DOE E3SM coupled model version 1: overview and evaluation at standard resolution. *J Adv Model Earth Syst* 11(7):2089–2129. <https://doi.org/10.1029/2018MS001603>
- Gulev SK, Thorne PW, Ahn J, Dentener FJ, Domingues CM, Gerland S, Gong D, Kaufman DS, Nnamchi HC, Quaas J, Rivera JA, Sathyendranath S, Smith SL, Trewin B, von Schuckmann K, Vose RS (2021) Changing state of the climate system. In: Masson-Delmotte V, Zhai P, Pirani A, Connors SL, Péan C, Berger S, Caud N, Chen Y, Goldfarb L, Gomis MI, Huang M, Leitzell K, Lonnoy E, Matthews JBR, Maycock TK, Waterfield T, Yelekçi O, Yu R, Zhou B (eds) *Climate change 2021: the physical science basis. Contribution of Working Group I to the Sixth Assessment Report of the Intergovernmental Panel on Climate Change*. Cambridge University Press, Cambridge, pp 287–422. <https://doi.org/10.1017/9781009157896.004>
- Herrera-Estrada JE, Martínez JA, Dominguez F, Findell KL, Wood EF, Sheffield J (2019) Reduced moisture transport linked to drought propagation across North America. *Geophys Res Lett* 46(10):5243–5253. <https://doi.org/10.1029/2019GL082475>
- Hersbach H, Bell B, Berrisford P, Hirahara S, Horányi A, Muñoz-Sabater J et al (2020) The ERA5 global reanalysis. *Q J R Meteorol Soc* 146(730):1999–2049. <https://doi.org/10.1002/qj.3803>
- Hoyos I, Dominguez F, Cañón-Barriga J, Martínez JA, Nieto R, Gimeno L, Dirmeyer PA (2018) Moisture origin and transport processes in Colombia, northern South America. *Clim Dyn* 50:971–990. <https://doi.org/10.1007/s00382-017-3653-6>
- IPCC (2021) Summary for policymakers. In: Masson-Delmotte V, Zhai P, Pirani A, Connors SL, Péan C, Berger S, Caud N, Chen Y, Goldfarb L, Gomis MI, Huang M, Leitzell K, Lonnoy E, Matthews JBR, Maycock TK, Waterfield T, Yelekçi O, Yu R, Zhou B (eds) *Climate change 2021: the physical science basis. Contribution of Working Group I to the Sixth Assessment Report of the Intergovernmental Panel on Climate Change*. Cambridge University Press, Cambridge, p 332. <https://doi.org/10.1017/9781009157896.001>
- Jiménez-Sánchez G, Markowski PM, Jewtoukoff V, Young GS, Stensrud DJ (2019) The Orinoco low-level jet: an investigation of its characteristics and evolution using the WRF model. *J Geophys Res Atmos* 124(20):10696–10711. <https://doi.org/10.1029/2019JD030934>
- Jiménez-Sánchez G, Markowski PM, Young GS, Stensrud DJ (2020) The Orinoco low-level jet: an investigation of its mechanisms of formation using the WRF model. *J Geophys Res Atmos* 125(13):e2020JD032810. <https://doi.org/10.1029/2020JD032810>
- Kelley M, Schmidt GA, Nazarenko LS, Bauer SE, Ruedy R, Russell GL et al (2020) GISS-E2.1: configurations and climatology. *J Adv Model Earth Syst* 12(8):e2019MS002025. <https://doi.org/10.1029/2019MS002025>
- Kendall MG (1948) Rank correlation methods. Charles Griffin & Co. Ltd, London, p 160
- Kodinariya T, Makwana P (2013) Review on determining of cluster in K-means clustering. *Int J Adv Res Comput Sci Manag Stud* 1:90–95
- Krishnan R, Swapna P, Choudhury AD, Narayansetti S, Prajeesh AG, Singh M et al (2021) The IITM Earth System Model (IITM-ESM). arXiv preprint [arXiv:2101.03410](https://arxiv.org/abs/2101.03410). <https://doi.org/10.48550/arXiv.2101.03410>
- Labar RJ, Douglas M, Murillo J, Mejia JF (2005) The Llanos low-level jet and its association with Venezuelan convective precipitation. *Weather* 98926:1–21
- Lee J, Kim J, Sun MA, Kim BH, Moon H, Sung HM et al (2020) Evaluation of the Korea meteorological administration advanced community earth-system model (K-ACE). *Asia-Pac J Atmos Sci* 56(3):381–395. <https://doi.org/10.1007/s13143-019-00144-7>
- Lee J-Y, Marotzke J, Bala G, Cao ZL, Corti S, Dunne JP, Engelbrecht F, Fischer E, Fyfe JC, Jones C, Maycock A, Mutemi J, Ndiaye O, Panickal S, Zhou T (2021) Future global climate: scenario-based projections and near-term information. In: Masson-Delmotte V, Zhai P, Pirani A, Connors SL, Péan C, Berger S, Caud N, Chen Y, Goldfarb L, Gomis MI, Huang M, Leitzell K, Lonnoy E, Matthews JBR, Maycock TK, Waterfield T, Yelekçi O, Yu R, Zhou B (eds) *Climate change 2021: the physical science basis. Contribution of Working Group I to the Sixth Assessment Report of the Intergovernmental Panel on Climate Change*. Cambridge University Press, Cambridge, pp 553–672. <https://doi.org/10.1017/9781009157896.006>
- Liu B, Tan X, Gan TY, Chen X, Lin K, Lu M, Liu Z (2020) Global atmospheric moisture transport associated with precipitation extremes: Mechanisms and climate change impacts. *Wiley Interdiscip Rev Water* 7(2):e1412. <https://doi.org/10.1002/wat2.1412>
- Llopart M, Simões Reboita M, Porfírio da Rocha R (2020) Assessment of multi-model climate projections of water resources over South America CORDEX domain. *Clim Dyn* 54(1):99–116. <https://doi.org/10.1007/s00382-019-04990-z>
- Loaiza-Cerón W, Andreoli RV, Kayano MT, Ferreira de Souza RA, Jones C, Carvalho LM (2020) The influence of the Atlantic multi-decadal oscillation on the Choco low-level jet and precipitation in Colombia. *Atmosphere* 11(2):174. <https://doi.org/10.3390/atmos11020174>
- Makinde AI, Abiodun BJ, James R, Washington R, Dyer E, Webb T (2022) How well do CMIP6 models simulate the influence of the West African westerly jet on Sahel precipitation? <https://doi.org/10.21203/rs.3.rs-1274137/v1>
- Mann HB (1945) Nonparametric tests against trend. *Econometrica* 13(3):245–259. <https://doi.org/10.2307/1907187>
- Martínez JA, Arias PA, Junquas C, Espinoza JC, Condom T, Dominguez F, Morales JS (2022) The Orinoco Low-level jet and the cross-equatorial moisture transport over tropical South America: lessons from Seasonal WRF simulations. *J Geophys Res Atmos* 127(3):e2021JD035603. <https://doi.org/10.1029/2021JD035603>

- Mauritsen T, Bader J, Becker T, Behrens J, Bittner M, Brokopf R et al (2019) Developments in the MPI-M earth system model version 1.2 (MPI-ESM1.2) and its response to increasing CO₂. *J Adv Model Earth Syst* 11(4):998–1038. <https://doi.org/10.1029/2018MS001400>
- Meinshausen M, Nicholls ZR, Lewis J, Gidden MJ, Vogel E, Freund M et al (2020) The shared socio-economic pathway (SSP) greenhouse gas concentrations and their extensions to 2500. *Geosci Model Dev* 13(8):3571–3605. <https://doi.org/10.5194/gmd-13-3571-2020>
- Mesa O, Urrea V, Ochoa A (2021) Trends of hydroclimatic intensity in Colombia. *Climate* 9(7):120. <https://doi.org/10.3390/cli9070120>
- Montoya GG, Pelkowski J, Eslava RJA (2001) Sobre los alisios del nordeste y la existencia de una corriente en el piedemonte oriental andino. *Revista de la Academia Colombiana de Ciencias Exactas Físicas y Naturales* 25(96): 363. <https://link.gale.com/apps/doc/A498583713/IFME?u=googlescholar&sid=bookmark-IFME&xid=2e07c8fa>
- Morales JS, Arias PA, Martínez JA, Durán-Quesada AM (2021) The role of low-level circulation on water vapour transport to central and northern South America: Insights from a 2D Lagrangian approach. *Int J Climatol* 41:E2662–E2682. <https://doi.org/10.1002/joc.6873>
- Munday C, Washington R, Hart N (2021) African low-level jets and their importance for water vapor transport and rainfall. *Geophys Res Lett* 48(1):e2020GL090999. <https://doi.org/10.1029/2020GL090999>
- Muñoz E, Busalacchi AJ, Nigam S, Ruiz-Barradas A (2008) Winter and summer structure of the Caribbean low-level jet. *J Clim* 21(6):1260–1276. <https://doi.org/10.1175/2007JCLI1855.1>
- Nieto R, Gallego D, Trigo R, Ribera P, Gimeno L (2008) Dynamic identification of moisture sources in the Orinoco basin in equatorial South America. *Hydrol Sci J* 53(3):602–617. <https://doi.org/10.1623/hysj.53.3.602>
- Olmo ME, Espinoza JC, Bettolli ML, Sierra JP, Junquas C, Arias PA et al (2022) Circulation patterns and associated rainfall over South Tropical South America: GCMs evaluation during the dry-to-wet transition season. *J Geophys Res Atmos*. <https://doi.org/10.1029/2022JD036468>
- Ortega G, Arias PA, Villegas JC, Marquet PA, Nobre P (2021) Present day and future climate over central and South America according to CMIP5/CMIP6 models. *Int J Climatol* 41(15):6713–6735. <https://doi.org/10.1002/joc.7221>
- Oscar L, Nzau MJ, Ellen D, Franklin O, Rachel J, Richard W, Tom W (2022) Characteristics of the Turkana low-level jet stream and the associated rainfall in CMIP6 models. *Clim Dyn* 11:1–17. <https://doi.org/10.1007/s00382-022-06499-4>
- Pak G, Noh Y, Lee MI, Yeh SW, Kim D, Kim SY et al (2021) Korea institute of ocean science and technology earth system model and its simulation characteristics. *Ocean Sci J* 56(1):18–45. <https://doi.org/10.1007/s12601-021-00001-7>
- Park S, Shin J, Kim S, Oh E, Kim Y (2019) Global climate simulated by the Seoul National University atmosphere model version 0 with a unified convection scheme (SAM0-UNICON). *J Clim* 32(10):2917–2949. <https://doi.org/10.1175/JCLI-D-18-0796.1>
- Poveda G, Mesa O (1999) La corriente de chorro superficial del Oeste (“del Chocó”) y otras dos corrientes de chorro en Colombia: climatología y variabilidad durante las fases del ENSO. *Revista Académica Colombiana De Ciencia* 23(89):517–528
- Poveda G, Jaramillo L, Vallejo LF (2014) Seasonal precipitation patterns along pathways of South American low-level jets and aerial rivers. *Water Resour Res* 50(1):98–118. <https://doi.org/10.1002/2013WR014087>
- Ramos AM, Nieto R, Tomé R, Gimeno L, Trigo RM, Liberato ML, Lavers DA (2016) Atmospheric rivers moisture sources from a Lagrangian perspective. *Earth System Dyn* 7(2):371–384. <https://doi.org/10.5194/esd-7-371-2016>
- Ramos AM, Blamey RC, Algarra I, Nieto R, Gimeno L, Tomé R et al (2019) From Amazonia to southern Africa: atmospheric moisture transport through low-level jets and atmospheric rivers. *Ann N Y Acad Sci* 1436(1):217–230. <https://doi.org/10.1111/nyas.13960>
- Reboita MS, da Rocha RP, Dias CG, Ynoue RY (2014) Climate projections for South America: RegCM3 driven by HadCM3 and ECHAM5. *Adv Meteorol*. <https://doi.org/10.1155/2014/376738>
- Rencher AC (2003) *Methods of multivariate analysis*, vol 492. Wiley
- Reyer CP, Adams S, Albrecht T, Baarsch F, Boit A, Canales Trujillo N et al (2017) Climate change impacts in Latin America and the Caribbean and their implications for development. *Reg Environ Change* 17(6):1601–1621. <https://doi.org/10.1007/s10113-015-0854-6>
- Riahi K, Van Vuuren DP, Kriegler E, Edmonds J, O’neillFujimori BCS et al (2017) The Shared Socioeconomic Pathways and their energy, land use, and greenhouse gas emissions implications: an overview. *Glob Environ Change* 42:153–168. <https://doi.org/10.1016/j.gloenvcha.2016.05.009>
- Rind D, Orbe C, Jonas J, Nazarenko L, Zhou T, Kelley M et al (2020) GISS Model E22: a climate model optimized for the middle atmosphere—model structure, climatology, variability, and climate sensitivity. *J Geophys Res Atmos* 125(10):e2019JD032204. <https://doi.org/10.1029/2019JD032204>
- Rodríguez-Gómez C, Echeverry G, Jaramillo A, Ladino LA (2022) The negative impact of biomass burning and the Orinoco low-level jet on the air quality of the Orinoco River Basin. *Atmósfera* 35(3):497–520. <https://doi.org/10.20937/ATM.52979>
- Rousseeuw PJ (1987) Silhouettes: a graphical aid to the interpretation and validation of cluster analysis. *J Comput Appl Math* 20:53–65. [https://doi.org/10.1016/0377-0427\(87\)90125-7](https://doi.org/10.1016/0377-0427(87)90125-7)
- Rueda C (2014) Caracterización de la Corriente en Chorro de Bajo Nivel de los Llanos Orientales Colombianos. [Master’s thesis, Dept. de Geociencias, Universidad Nacional de Colombia] https://www.simfac.mil.co/sites/default/files/doctrinamet/2022-03/Diana%20Rueda%20Dimate_Tesis%20Maestr%C3%ADa%20UNAL_0.pdf
- Ruiz-Vásquez M, Arias PA, Martínez JA, Espinoza JC (2020) Effects of Amazon basin deforestation on regional atmospheric circulation and water vapor transport towards tropical South America. *Clim Dyn* 54:4169–4189. <https://doi.org/10.1007/s00382-020-05223-4>
- San José JJ, Montes R, Mazorra M (1998) The nature of savanna heterogeneity in the Orinoco Basin. *Glob Ecol Biogeogr Lett* 7(6):441–455
- Segura H, Espinoza JC, Junquas C, Lebel T, Vuille M, Garreaud R (2020) Recent changes in the precipitation-driving processes over the southern tropical Andes/western Amazon. *Clim Dyn* 54(5):2613–2631. <https://doi.org/10.1007/s00382-020-05132-6>
- Seland Ø, Bentsen M, Olivie D, Toniazzo T, Gjermundsen A, Graff LS et al (2020) Overview of the Norwegian Earth System Model (NorESM2) and key climate response of CMIP6 DECK, historical, and scenario simulations. *Geosci Model Devel* 13(12):6165–6200. <https://doi.org/10.5194/gmd-13-6165-2020>
- Seneviratne SI, Zhang X, Adnan M, Badi W, Dereczynski C, Di Luca A, Ghosh S, Iskandar I, Kossin J, Lewis S, Otto F, Pinto I, Satoh M, Vicente-Serrano SM, Wehner M, Zhou B (2021) Weather and climate extreme events in a changing climate. In: Masson-Delmotte V, Zhai P, Pirani A, Connors SL, Péan C, Berger S, Caud N, Chen Y, Goldfarb L, Gomis MI, Huang M, Leitzell K, Lonnoy E, Matthews JBR, Maycock TK, Waterfield T, Yelekçi O, Yu R, Zhou B (eds) *Climate change 2021: the physical science basis. Contribution of Working Group I to the Sixth Assessment Report of the Intergovernmental Panel on Climate Change*. Cambridge

- University Press, Cambridge, pp 1513–1766. <https://doi.org/10.1017/9781009157896.013>
- Sepulchre P, Caubel A, Ladant JB, Bopp L, Boucher O, Braconnot P et al (2020) IPSL-CM5A2—an earth system model designed for multimillennial climate simulations. *Geosci Model Dev* 13(7):3011–3053. <https://doi.org/10.5194/gmd-2019-332>
- Sierra JP, Arias PA, Vieira SC, Agudelo J (2018) How well do CMIP5 models simulate the low-level jet in western Colombia? *Clim Dyn* 51(5):2247–2265. <https://doi.org/10.1007/s00382-017-4010-5>
- Sierra JP, Arias PA, Durán-Quesada AM, Tapias KA, Vieira SC, Martínez JA (2021a) The Choco low-level jet: past, present and future. *Clim Dyn* 56(7):2667–2692. <https://doi.org/10.1007/s00382-020-05611-w>
- Sierra JP, Junquas C, Espinoza JC, Segura H, Condom T, Andrade M, Sicart JE (2021b) Deforestation impacts on Amazon-Andes hydroclimatic connectivity. *Clim Dyn*. <https://doi.org/10.1007/s00382-021-06025-y>
- Sierra JP, Espinoza JC, Junquas C et al (2023) Impacts of land-surface heterogeneities and Amazonian deforestation on the wet season onset in southern Amazon. *Clim Dyn*. <https://doi.org/10.1007/s00382-023-06835-2>
- Stensrud DJ (1996) Importance of low-level jets to climate: a review. *J Clim* 9(8):1698–1711. [https://doi.org/10.1175/1520-0442\(1996\)009%3c1698:IOLLJT%3e2.0.CO;2](https://doi.org/10.1175/1520-0442(1996)009%3c1698:IOLLJT%3e2.0.CO;2)
- Stouffer RJ (2019) UA MCM-UA-1-0 model output prepared for CMIP6 CMIP historical, Earth System Grid Federation. <https://doi.org/10.22033/ESGF/CMIP6.8888>
- Swart NC, Cole JN, Kharin VV, Lazare M, Scinocca JF, Gillett NP et al (2019) The Canadian earth system model version 5 (CanESM5.0.3). *Geosci Model Dev* 12(11):4823–4873. <https://doi.org/10.5194/gmd-12-4823-2019>
- Tarek M, Brissette FP, Arsenault R (2020) Evaluation of the ERA5 reanalysis as a potential reference dataset for hydrological modelling over North America. *Hydrol Earth Syst Sci* 24(5):2527–2544. <https://doi.org/10.5194/hess-24-2527-2020>
- Tatebe H, Ogura T, Nitta T, Komuro Y, Ogochi K, Takemura T et al (2019) Description and basic evaluation of simulated mean state, internal variability, and climate sensitivity in MIROC6. *Geosci Model Dev* 12(7):2727–2765. <https://doi.org/10.5194/gmd-12-2727-2019>
- Taylor KE (2001) Summarizing multiple aspects of model performance in a single diagram. *J Geophys Res Atmos* 106(D7):7183–7192
- Torrealba ER, Amador JA (2010) La corriente en chorro de bajo nivel de los Llanos Venezolanos de Sur América. *Revista De Climatología* 10:1–20 (ISSN 1578-8768)
- Torres-Alavez JA, Das S, Corrales-Suastegui A, Coppola E, Giorgi F, Raffaele F et al (2021) Future projections in the climatology of global low-level jets from CORDEX-CORE simulations. *Clim Dyn* 57(5):1551–1569. <https://doi.org/10.1007/s00382-021-05671-6>
- Urrea V, Ochoa A, Mesa O (2019) Seasonality of rainfall in Colombia. *Water Resour Res* 55(5):4149–4162. <https://doi.org/10.1029/2018WR023316>
- Valencia J, Mejía JF (2022) Projected changes of day-to-day precipitation and choco low-level jet relationships over the far Eastern Tropical Pacific and Western Colombia from two CMIP6 GCM models. *Atmosphere* 13(11):1776. <https://doi.org/10.3390/atmos13111776>
- Volodin E, Gritsun A (2018) Simulation of observed climate changes in 1850–2014 with climate model INM-CM5. *Earth Syst Dyn* 9(4):1235–1242. <https://doi.org/10.5194/esd-9-1235-2018>
- Wang C (2007) Variability of the Caribbean low-level jet and its relations to climate. *Clim Dyn* 29(4):411–422. <https://doi.org/10.1007/s00382-007-0243-z>
- Ward JH Jr (1963) Hierarchical grouping to optimize an objective function. *J Am Stat Assoc* 58(301):236–244
- Whyte FS, Taylor MA, Stephenson TS, Campbell JD (2007) Features of the Caribbean low-level jet. *Int J Climatol A J R Meteor Soc* 28(1):119–128. <https://doi.org/10.1002/joc.1510>
- Wilks DS (2006) *Statistical methods in the atmospheric sciences*, 2nd edn. Academic Press, London, p 627
- Wu T, Lu Y, Fang Y, Xin X, Li L, Li W et al (2019) The Beijing Climate Center climate system model (BCC-CSM): the main progress from CMIP5 to CMIP6. *Geosci Model Dev* 12(4):1573–1600. <https://doi.org/10.5194/gmd-12-1573-2019>
- Wu T, Zhang F, Zhang J, Jie W, Zhang Y, Wu F et al (2020) Beijing Climate Center Earth System Model version 1 (BCC-ESM1): model description and evaluation of aerosol simulations. *Geoscientific Model Development* 13(3):977–1005. <https://doi.org/10.5194/gmd-13-977-2020>
- Xin-Yao RONG, Jian LI, Hao-Ming CHEN, Yu-Fei XIN, Jing-Zhi SU, Li-Juan HUA (2019) Introduction of CAMS-CSM model and its participation in CMIP6. *Adv Clim Change Res* 15(5):540. <https://doi.org/10.12006/j.issn.1673-1719.2019.186>
- Yang D, Yang Y, Xia J (2021) Hydrological cycle and water resources in a changing world: a review. *Geogr Sustain* 2(2):115–122. <https://doi.org/10.1016/j.geosus.2021.05.003>
- Yepes J, Poveda G, Mejía JF, Moreno L, Rueda C (2019) Choco-jex: a research experiment focused on the Chocó low-level jet over the far eastern Pacific and western Colombia. *Bull Am Meteor Soc* 100(5):779–796. <https://doi.org/10.1175/BAMS-D-18-0045.1>
- Yukimoto S, Kawai H, Koshiro T, Oshima N, Yoshida K, Urakawa S et al (2019) The Meteorological Research Institute Earth System Model version 2.0, MRI-ESM2.0: description and basic evaluation of the physical component. *J Meteorol Soc Jpn Ser II*. <https://doi.org/10.2151/jmsj.2019-051>
- Zaninelli PG, Menéndez CG, Falco M, López-Franca N, Carril AF (2019) Future hydroclimatological changes in South America based on an ensemble of regional climate models. *Clim Dyn* 52(1):819–830. <https://doi.org/10.1007/s00382-018-4225-0>
- Ziehn T, Chamberlain MA, Law RM, Lenton A, Bodman RW, Dix M et al (2020) The Australian earth system model: ACCESS-ESM1.5. *J Southern Hemisphere Earth Syst Sci* 70(1):193–214. <https://doi.org/10.1071/ES19035>

Publisher's Note Springer Nature remains neutral with regard to jurisdictional claims in published maps and institutional affiliations.